LA-UR-20-24715
Approved for public release; distribution is unlimited.

Title: Comparison of Modeled to Measured Spectra using MCNP and GADRAS to Benchmark and Contrast Modeling Limitations

Author(s): Stults, Katrina Ann
James, Michael R.
Lombardi, Marcie
Klasky, Marc Louis

Intended for: Report

Issued: 2020-06-29

Comparison of Modeled to Measured Spectra using MCNP and GADRAS to Benchmark and Contrast Modeling Limitations

Contents

Figures

Tables

1. Introduction

The desire to improve nuclear material detection through portal monitors and other low resolution detectors has led to interest in benchmarking the performance of radiation transport codes. These codes can be used to generate a variety and quantity of spectra that may be cost prohibitive to measure directly. Particular characteristics of typical detection scenarios were isolated to compare the performance of radiation transport codes to laboratory experiments.

These benchmark experiments were performed to validate simulations in a number of key areas. These experiments included high areal density configurations in both one- and three-dimensional configurations. In addition, off-angle measurements were conducted to investigate the impact of detector response assumptions on complex geometries, for example where an unknown source is not physically collocated with an apparent hot spot. Furthermore, by examining both simple shielding and backscatter configurations, isolation of the scatter emanating from the object and environmental background scatter contributions to the spectra could be elucidated.

A series of experiments were performed in which the order of shielding layers and the thickness were evaluated to examine the ability of the simulations to address these variables. Experiments with increasing thickness of polyethylene around a neutron source also allows for examinations of the ability of the transport simulations to properly model n,γ reactions. Finally, depleted uranium (DU) measurements have more complicated spectra than the cobalt-60 and consequently allow for investigations into the ability of transport simulations to model self-shielding.

In each case, the results of the experiments were compared to MCNP simulations to judge the performance of the code, as was done previously with GADRAS 18.7.9 simulations [7].

All of the benchmark measurements were taken with a liquid nitrogen cooled 140% high purity germanium (HPGe) detector with a bismuth collimator that had the front tin filter removed. The measurement location and detector configuration were subsequently used for all experimental configurations.

The remainder of this report details the experimental measurements, Section 2 and the MCNP model, Section 3. Comparisons between the experimental results and MCNP-generated spectra are performed, Section 4. Section 5 compares the results obtained with MCNP with the previously reported results obtained with GADRAS [2]. Finally, Section 6 presents the conclusions.

2. Experimental Details

The experimental details were discussed in a previous report [7]. All measurements were performed with a liquid nitrogen cooled 140% efficient HPGe detector, identified as detector S, at Los Alamos National Laboratory in the south hot cell in 2322-303. The bismuth collimator was always used, with the front tin filter removed. This was to cut down scattered radiation from the room without blocking direct low energy gamma rays from reaching the detector. The low energy region is often challenging to replicate when performing simulations. The height of the center of each source configuration was set at 87.5 cm to match the height of the center of the HPGe detector. The characterization measurements and all subsequent configurations were at a distance of 2 m from the detector face to the center of the

source configuration. A standard suite of sources was used to characterize the detector and build the detector models:

- Am-241, 101 uCi
- Ba-133, 100 uCi
- Cs-137, 154 uCi
- Co-60, 60 uCi
- U-232, 45 uCi

Experimental measurements used a Co-60 source of about 120 uCi (activity on each day of measurement is given in the section detailing those measurements). A larger 4.9 mCi Co-60 source, a 57 uCi Cf-252 source, and a set of nesting DU spheres were also utilized in the experimental investigations. In the remainder of this Section the experimental details of the configurations are provided.

2.1. High Areal Density Shielding

For the first series of measurements taken, a set of spectra was collected with shielding configurations (both 1-D and 3-D), ranging in areal density from 47.6 to 80 g/cm^2. A cobalt-60 source, activity 4.9 mCi, was placed in each configuration, using foam as needed, to center the source.

The first configuration examined was an iron box with 4-inch thick walls, resulting in an areal density of 80 g/cm^2. The central void was 4 inches square, and the outer dimension was 12 inches. Figure 1 shows this configuration.

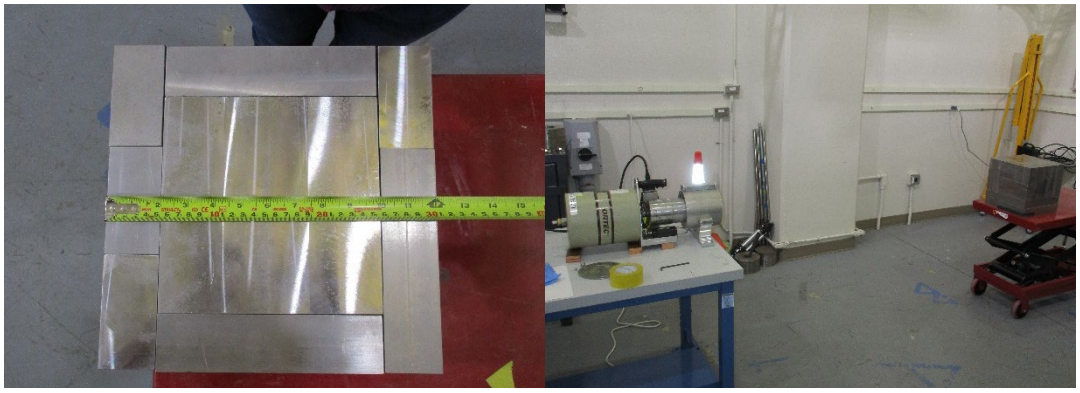

Figure 1. Experimental configuration for iron box

The next configuration examined had an areal density (58 g/cm^2). This configuration had a three-dimensional box consisting of 2 inches of lead, also with an internal void of 4 inches (8 inches external dimensions). This configuration is shown in Figure 2.

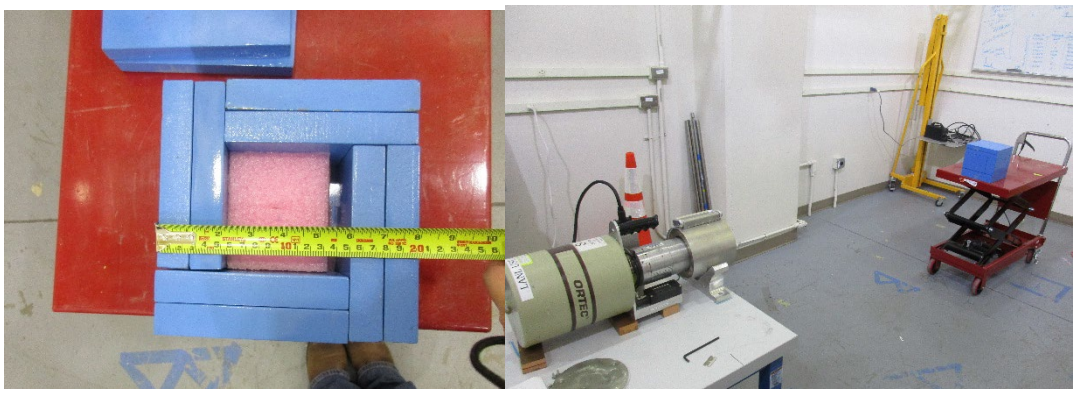

Figure 2. Experimental configuration for lead box

The third shielding configuration had an areal density of 58 g/cm^2. This configuration consisted of a lead sphere, a one-dimensional analog of the 2-inch lead box, and also had an internal void diameter of 4 inches and outer diameter of 8 inches. Figure 3 shows photos of this configuration.

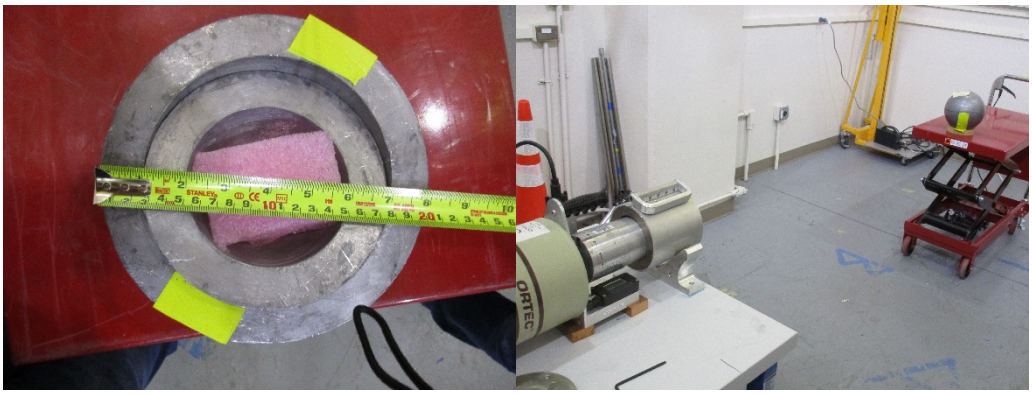

Figure 3. Experimental configuration for lead sphere

The final areal density configuration (AD=47.6 g/cm^2) consisted of a one-inch lead sphere (inner diameter of 5 inches, outer diameter of 7 inches) inside of 4 inches of mock high explosives (MHE) (outer diameter of 16 inches). Photos of this configuration are shown in Figure 4.

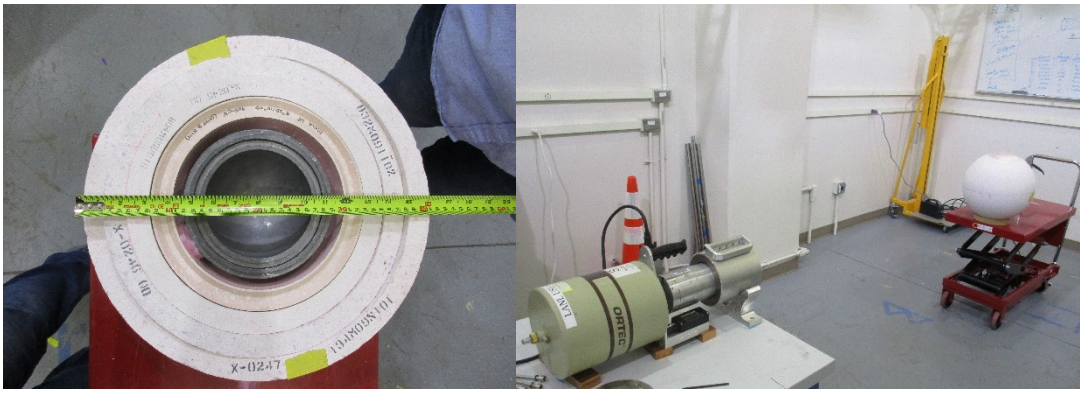

Figure 4. Experimental configuration for lead sphere surrounded by mock high explosives

2.2. Offsets

To simulate a source moving past the detector's field of view, a series of off-angle or off-set measurements were taken. The center (distance of closest approach) was the same 2 m as the detector characterization measurements. On a straight line perpendicular to the detector, measurements were taken every 50 cm from the center, with the absolute source-detector distance increasing as the source moved farther from the detector centerline. Due to constraints of the room, measurements were taken out to 200 cm. The left-most measurement (denoted L-200) was 28 cm from the room wall, and the right-most measurement (denoted R-200) was 124 cm from the opposite room wall.

2.3. Scatter

This series of configurations was designed to break the iron box described in section 2.1 into its component pieces. For the shielded configuration, denoted as 'scatter' representing the front of the box, the same source that was placed in the box (Co-60, activity 4.9 mCi) was placed 2 inches behind a 4-inch thick 8 inch square slab of the same material used to build the box.

An identical 'scatter' configuration, resembling only the front face of the iron box, was also measured using a 116 uCi source. This smaller source was used for the 'backscatter' configuration, representing the back face of the box. A smaller source was required for the backscatter configuration so the detector would not be swamped by the direct gamma rays from the unshielded 4.9 mCi source.

2.4. Order of Shielding

Two configurations were examined to determine the impact of shielding order. Both configurations utilized a Co-60 (117.6 uCi) source within a 4-inch inner void surrounded by 2 inches of iron and 2 inches of polyethylene with an outer wall of 12 inches square. The difference between the two is the order of the shielding material: polyethylene nested in iron and iron nested in polyethylene, as depicted in Figure 5.

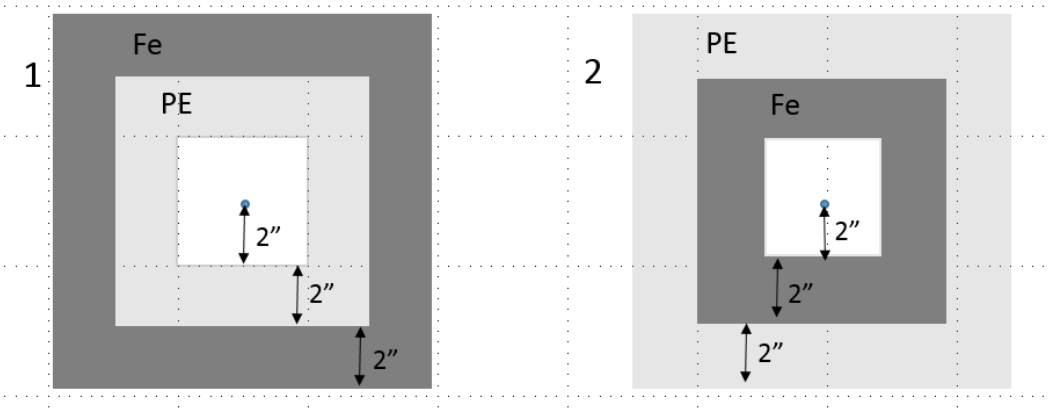

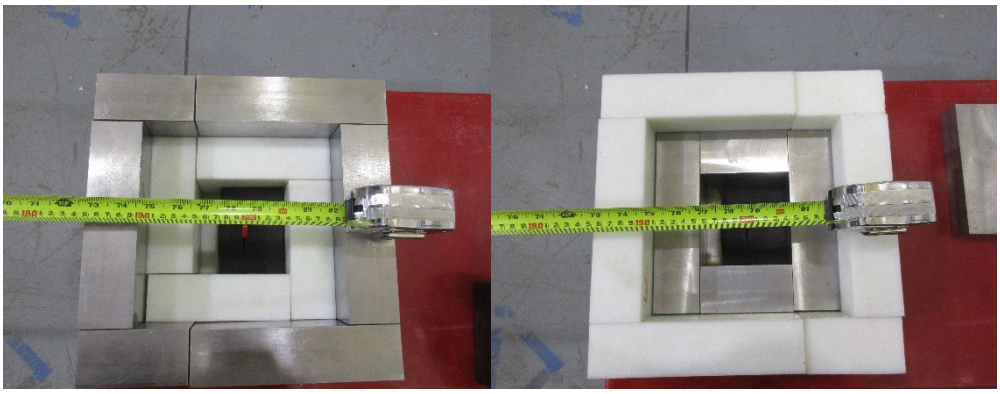

Figure 5. Schematics and photos of the nested iron and polyethylene configurations

2.5. Increasing Shielding Thickness

This series of measurements used a set of polyethylene shells with 4 inch inner void diameters and outer diameters of 9 inches, 11 inches, and 13 inches for wall thicknesses of 2.5, 3.5, and 4.5 inches, as shown in Figure 6, in addition to a measurement obtained with a bare source. This set of experiments utilized two different sources Co-60 (116.7 uCi), as well as Cf-252 (57.1 uCi).

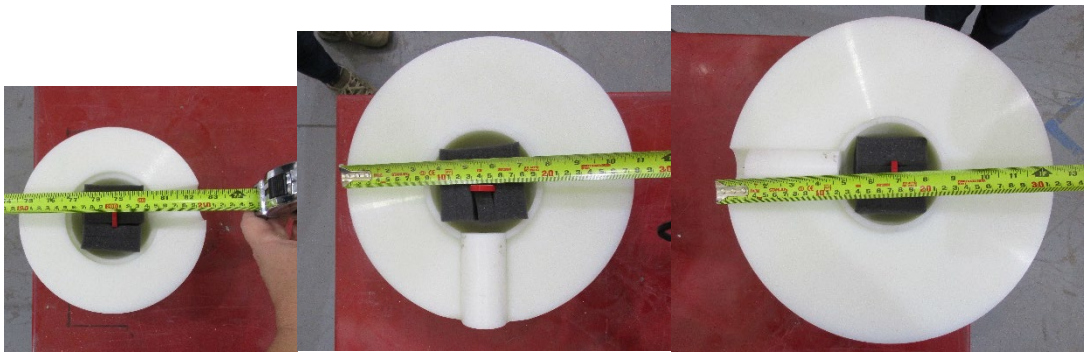

Figure 6. Photos of 9, 11, and 13 inch polyethylene shells

2.6. DU Shells

In addition to the Co-60 and Cf-252 sources, a series of DU spheres were utilized to perform experimental measurements. The nesting set of depleted uranium consists of a solid center sphere and 8 shells. First the center ball and half of the shells were nested to create a sphere with a 4 inch outer diameter. Adding the remaining shells created a sphere with a 6 inch outer diameter. The sphere and shells for these configurations are shown in Figure 7 prior to final assembly. The 6 inch sphere was also measured in an iron shell 1.25 inches thick with a 6.5 inch internal diameter. A photo of this configuration is shown in Figure 8.

Figure 7. Sphere and nesting shells of DU to make 4 inch and 6 inch spheres

Figure 8. The nested DU sphere and shells surrounded by 1.25 inches of iron

2.7. Offset and Angles With and Without Bi Side Shield

A series of measurements was taken to evaluate the performance of the simulations to model sources at off-angle source locations. In addition the performance with and without the Bi side shield was assessed. Measurements were taken with and without the Bi when the detector was 2 m from the side of the detector, 90° from the plane of the detector. In this configuration, no gamma rays enter the face of the detector; all gamma rays enter through the side. In addition, measurements were taken that directly mimic the offset measurements discussed in section 2.2 but the Bi was removed.

3. MCNP model

There have been many efforts to model HPGe gamma detectors with MCNP [4-6]. In this work, we follow the same general methodology using the Pulse Height Tally in MCNP to model the gamma spectrum from sources in various configurations.

To properly model the detector response, it was necessary to construct an accurate MCNP model of the detector geometry. Using the manufacturer specification sheet, a physical match to the detector was created in MCNP. A model of the room environment was also created, primarily the concrete wall and the tables for the sources and detector. MCNP 6.2 [1] with the MCPLIB84 libraries was used for the simulations.

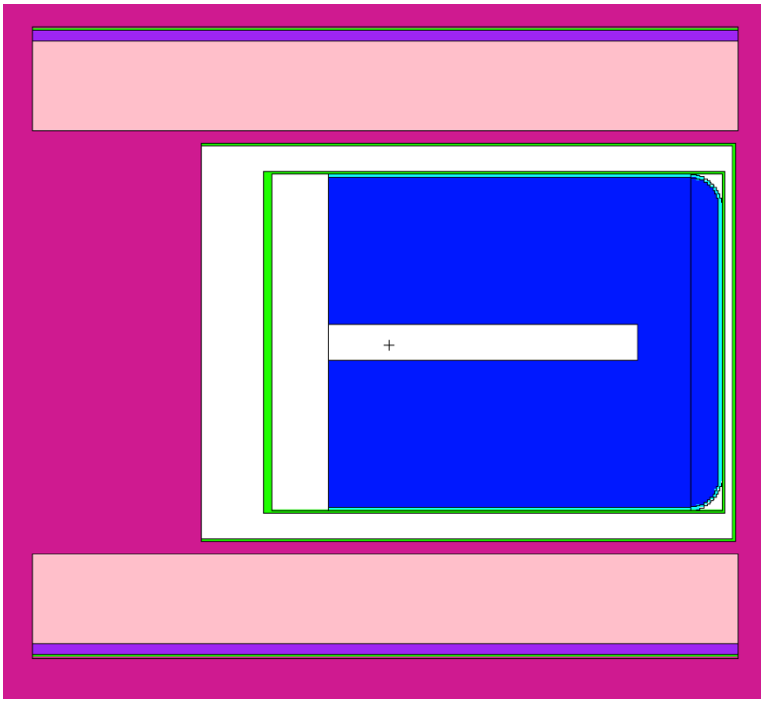

Figure 9. Side view of MCNP detector model with surrounding Bi side shield

Initially, the model was tested using both photon-only transport and photon-electron transport. Given the physical scale of the detector, the range of the electrons are relatively in comparison to those of the photons. Consequently, it was expected that using electron transport would have a negligible effect and allow for reduced computational time. To confirm this assumption, test runs were performed using identical configurations of Co-60 source 2m from the front face. Using the full-energy peaks as a comparison, the two runs differed by <1%. On this basis, it was decided to do all simulations using photon-only mode in MCNP.

The sources used in the detector calibration (Am241, Ba133, Eu152, Ho166m, Th228, Cs137, Co60, U232 were created in an MCNP deck with the detector model. The yields of the peaks were tallied in the model using an F8 tally were compared to the experimental values. Based on the observed differences, a response function was created from the observed differences in the model and this function was applied to the output tally spectrum through the use of the EM tally multiplier. This multiplier adjusted the magnitude of the detector response in MCNP to match the experimentally observed values. This factor accounts for mechanisms in the detector related to the physics of charge gathering and efficiency of the electronics.

Table 1. Lines Used for MCNP Response of Detector

Energy(keV)	Measured Co	MCNP Counts	Error	Ratio
59.5	62342	6.48E+04	1.86E-02	9.63E-01
238.6	31201	4.13E+04	1.22E-02	7.56E-01
276.4	5452	7.25E+03	1.23E-02	7.52E-01
302.9	13694	1.75E+04	1.27E-02	7.84E-01
356.0	42749	5.61E+04	1.31E-02	7.62E-01
383.8	6114	7.66E+03	1.34E-02	7.98E-01
583.2	16039	2.08E+04	1.44E-02	7.72E-01
661.7	70361.8	9.20E+04	1.48E-02	7.65E-01
1173.2	25606	3.53E+04	1.62E-02	7.26E-01
1332.5	24528	3.24E+04	1.69E-02	7.56E-01
2614.4	9658	1.27E+04	2.00E-02	7.59E-01

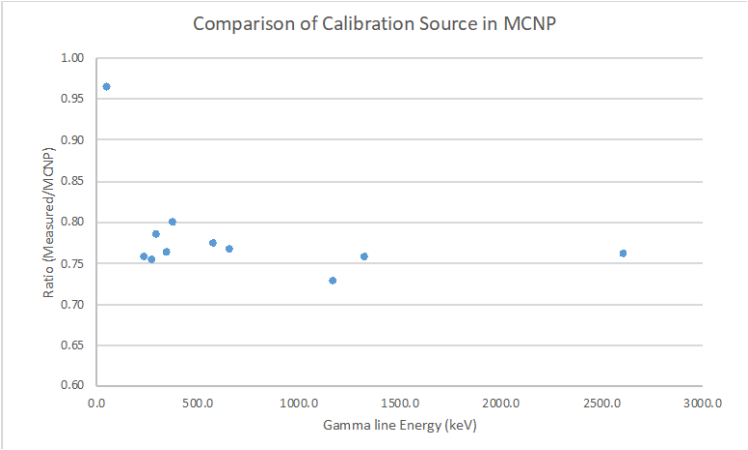

Figure 10: MCNP Response function as a function of energy

One additional aspect of the detector performance was determined using a best-fit Gaussian broadening set of parameters. Based on initial measurements of the Co-60 source, a fitting function was developed to match the measured the peak widths as a function of energy. The MCNP function parameters used were: geb 1.10E-3 7.7E-4 3.0.

The off-angle response of the detector was not characterized for other source positions. For all cases reported here, including the off-angle experiments, the response function (in the form of the tally multiplier) was the one computed from the source position in front of the detector. Also, for all measurements (except for the last set) a Bismuth shield was in place around the detector can to reduce off-angle contributions. Uncertainties in the true detector response, dead-layer thicknesses, Bi shield construction and other factors all contribute to uncertainty in modeling the detector response at low-energies and off-angle measurements. This assumption holds true if the charge-gathering inefficiencies in the detector are homogenous and not concentrated in one physical area. The MCNP simulations still

compute the consequences of oblique positioning of the source and the effect from the altered view factor on detector performance.

4. MCNP Model Comparisons

The experiments were conducted over the course of several months and were followed by the modeling for each configuration. The general basis for comparison is the modeled spectrum produced by MCNP given the inputs of the source type and strength, modeling configuration and the previously determined detector response in MCNP. An overall spectrum comparison will be given along with individual peak comparisons for some cases. For the comparisons, the background has been subtracted from the measurements and compared to the MCNP simulations.

4.1. High Areal Density Shielding

For this set of configurations, the areal density, shielding material, and geometry change. Table 2 summarized the comparison between the measured and modeled spectra. For the highest areal density, the thick iron box, MCNP over predicted the peak area slightly. For both the lead box and lead sphere, the peak areas are slightly under predicted. In the case of the two materials, lead and MHE, the peak areas were considerably under predicted. Based on the average percent difference, MCNP under predicts the continuum for all cases. More than half of the channels for the lead box and lead sphere and over 90% of the channels for the lead-MHE spheres differed by more than 3 sigma. There is very little difference between the lead box and lead sphere with the same areal density across all parameters. See Figures 11-14 for overlays of the measured spectra and MCNP modeled spectra, with close-ups of the peaks inset.

Table 2. Quantitative Comparison between Measured and Synthetic Spectra- High Areal Density Shielding Measurements

Config	Absolute % Difference	Average % Difference	Chi Square	% More than 3 σ Difference	Gamma cps % Difference	% Difference, 1173 keV peak	% Difference, 1332 keV peak
Fe box (AD=80)	12.4%	-6.4%	6.58	17.5%	-4.6%	2.4%	6.1%
Pb box (AD=58)	19.5%	-17.7%	12.73	52.2%	-15.3%	-9.9%	-4.9%
Pb sphere (AD=58)	20.5%	-18.7%	17.17	59.7%	-16.3%	-6.9%	-2.0%
Pb-MHE sphere (AD=47.6)	22.6%	-18.7%	62.02	93.4%	-11.1%	-25.0%	-19.8%

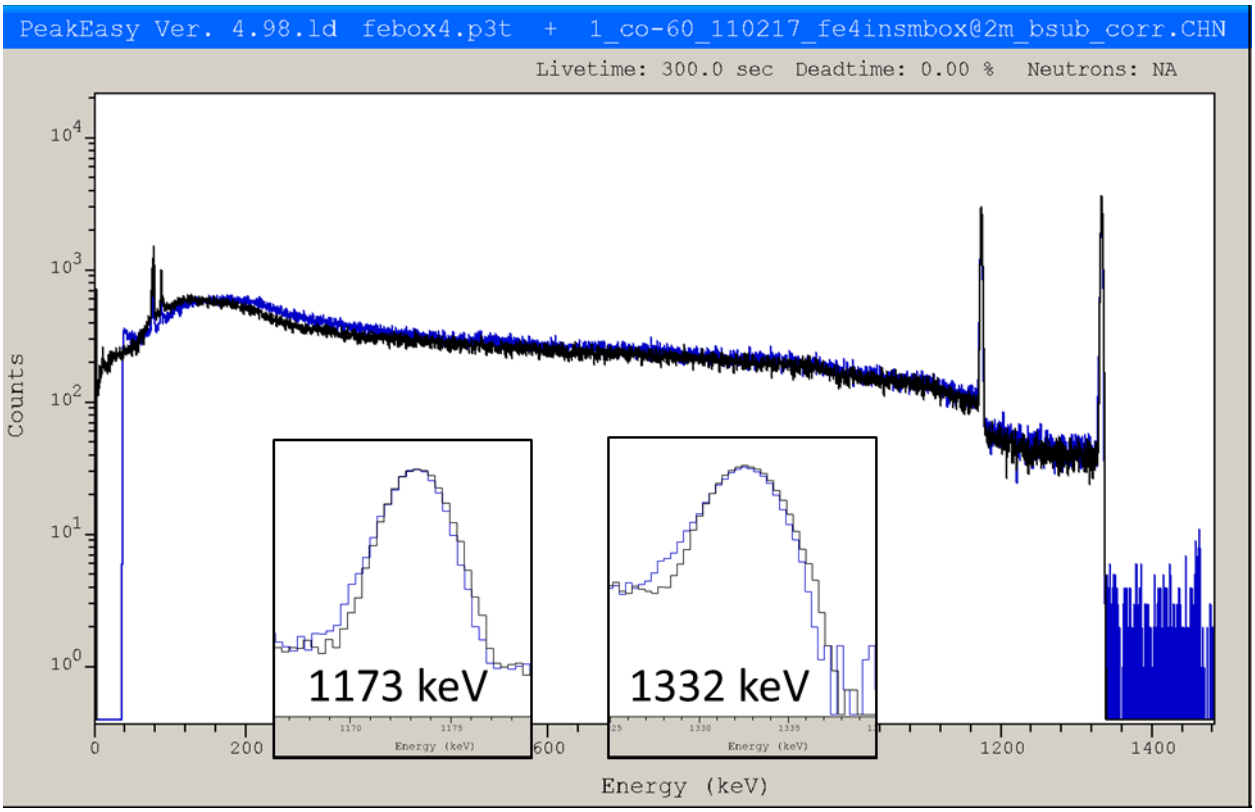

Figure 11. Spectra overlay, Fe- 4” box, Measured (Blue) vs Synthetic (Black) with peaks inset

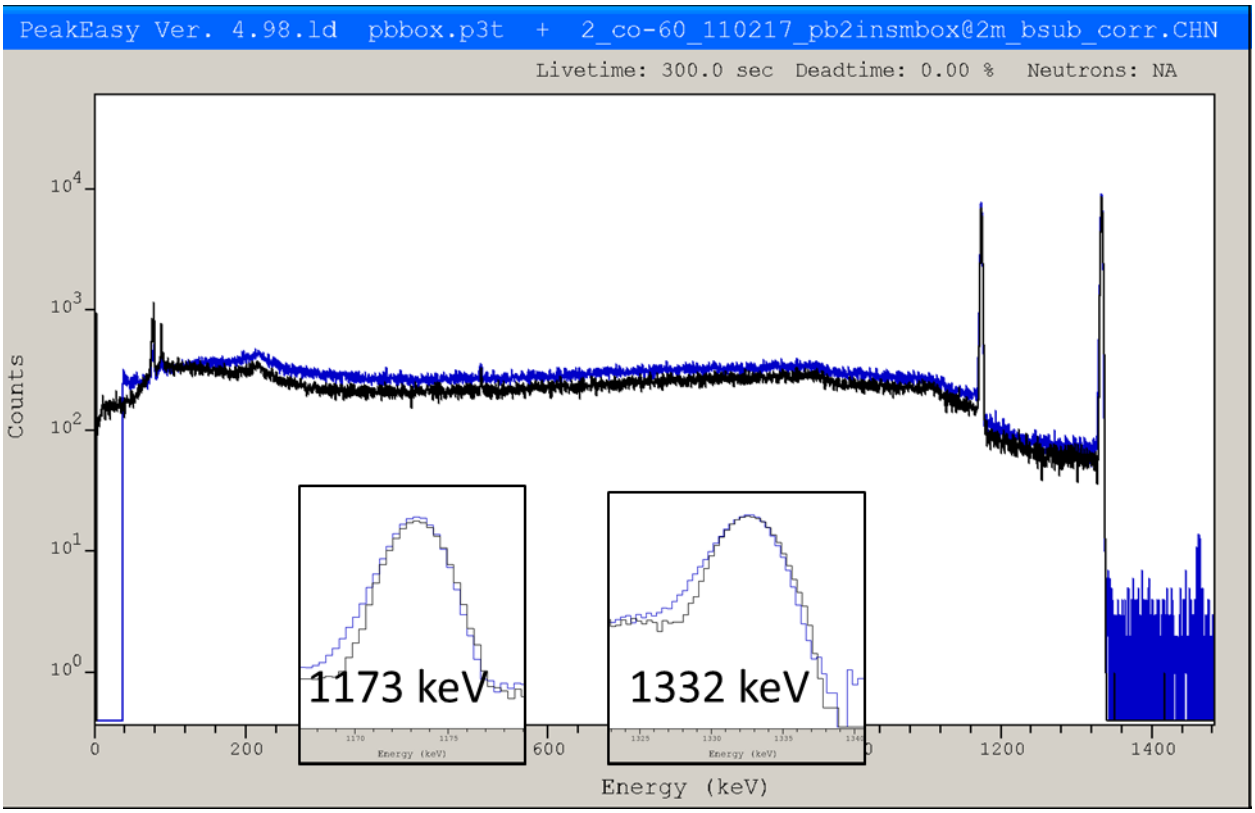

Figure 12. Spectra overlay, Pb- 2” box, Measured (Blue) vs Synthetic (Black) with peaks inset

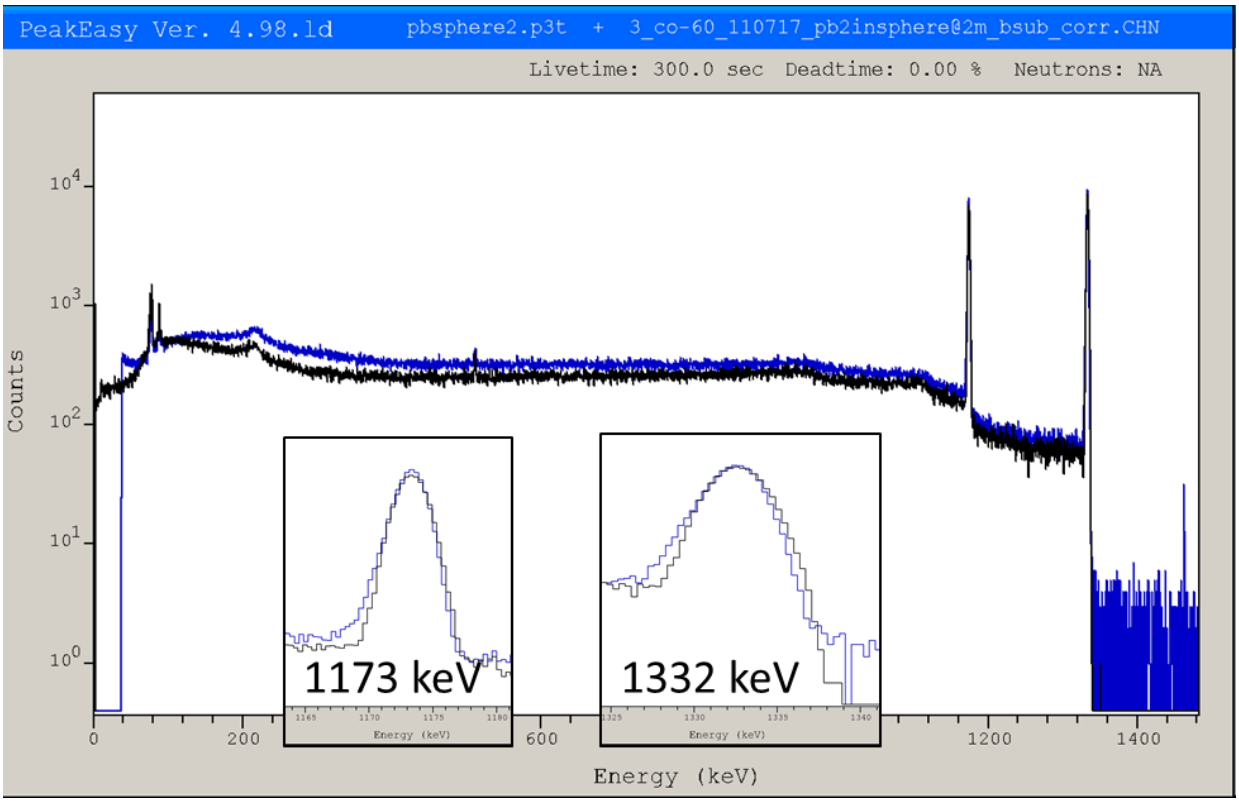

Figure 13. Spectral overlay, Pb- 2” sphere, Measured (Blue) vs Synthetic (Black) with peaks inset

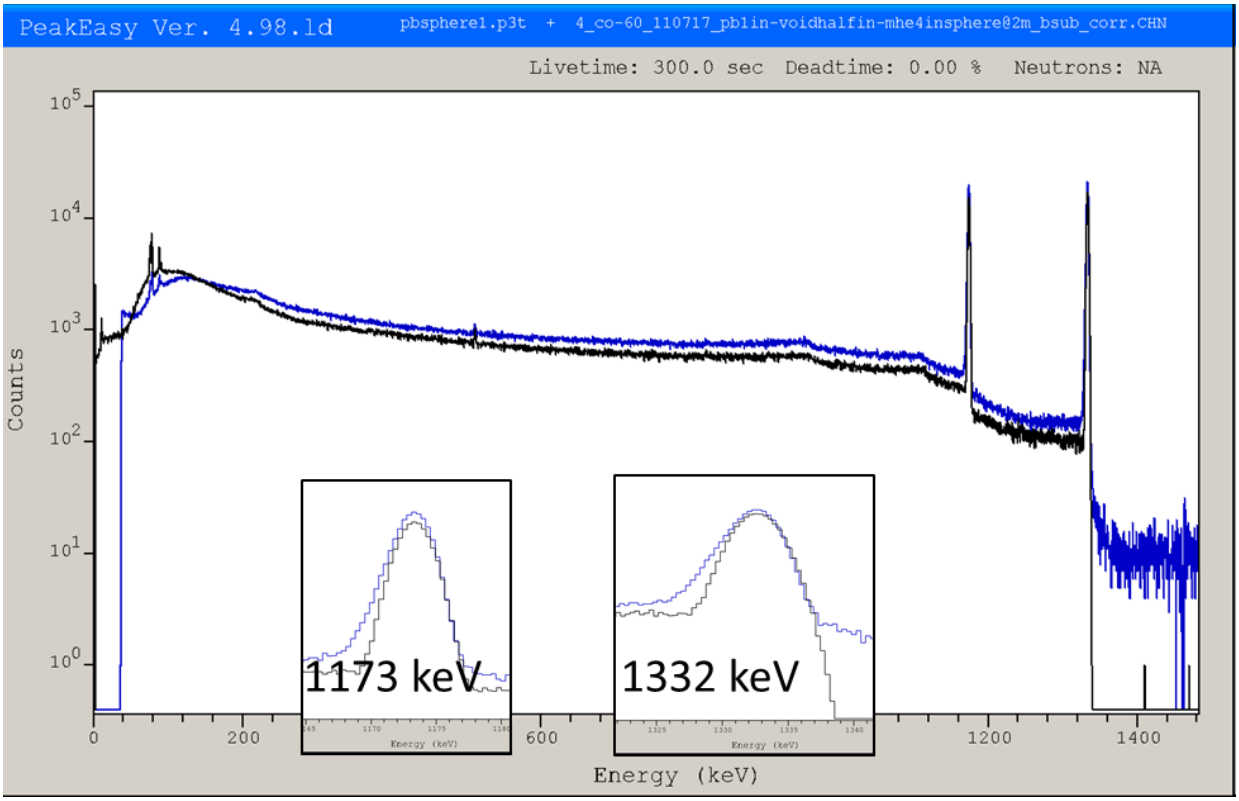

Figure 14. Spectra overlay, Pb- 2” sphere in MHE- 4” sphere, Measured (Blue) vs Synthetic (Black) with peaks inset

4.2. Offsets

A series of measurements were made where the source was translated, 50 cm at a time, along a line 2 m from and perpendicular to the detector. Table 3 summarized the comparison between measured and MCNP spectra. For the center and 50 cm offset measurements, the model predicts the peak areas quite well, but the continua are under predicted. At 100 cm and 150 cm, the continuum is still under predicted, but the peak areas are over predicted by more than 10%. At the farthest offset, 200 cm (45° angle), the peaks are over predicted by up to 20%. The detector response is changing in a way not predicted by the MCNP model. Figures 15-17 show the overlaid spectra for both extremes and the center position. Figure 18 compares the peak area for both photopeaks for measured and synthetic data at each offset position, which clearly shows the under prediction trend.

Table 3. Quantitative Comparison between Measured and Synthetic Spectra- Offset Measurements

Config	Absolute % Difference	Average % Difference	Chi Square	% More than 3 σ Difference	Gamma cps % Difference	% Difference, 1173 keV peak	% Difference, 1332 keV peak
Left- 200 cm 45°	25.7%	-6.2%	2.18	3.2%	-1.0%	11.4%	18.4%
Left- 150 cm 37°	23.1%	-10.5%	2.47	3.6%	-5.1%	7.1%	13.6%
Left- 100 cm 27°	22.6%	-14.5%	3.24	4.7%	-7.6%	5.2%	10.2%
Left- 50 cm 14°	22.1%	-18.2%	3.90	7.2%	-10.4%	1.1%	6.6%
Center	25.5%	-22.4%	5.11	12.9%	-14.5%	-1.6%	2.6%
Right- 50 cm 14°	23.4%	-19.7%	4.42	8.8%	-12.2%	-1.0%	4.0%
Right- 100 cm 27°	22.3%	-16.0%	3.38	5.0%	-8.6%	3.4%	10.7%
Right- 150 cm 37°	24.5%	-12.6%	2.66	4.2%	-7.9%	4.4%	12.4%
Right- 200 cm 45°	26.9%	-7.7%	2.19	3.0%	-4.2%	11.2%	20.3%

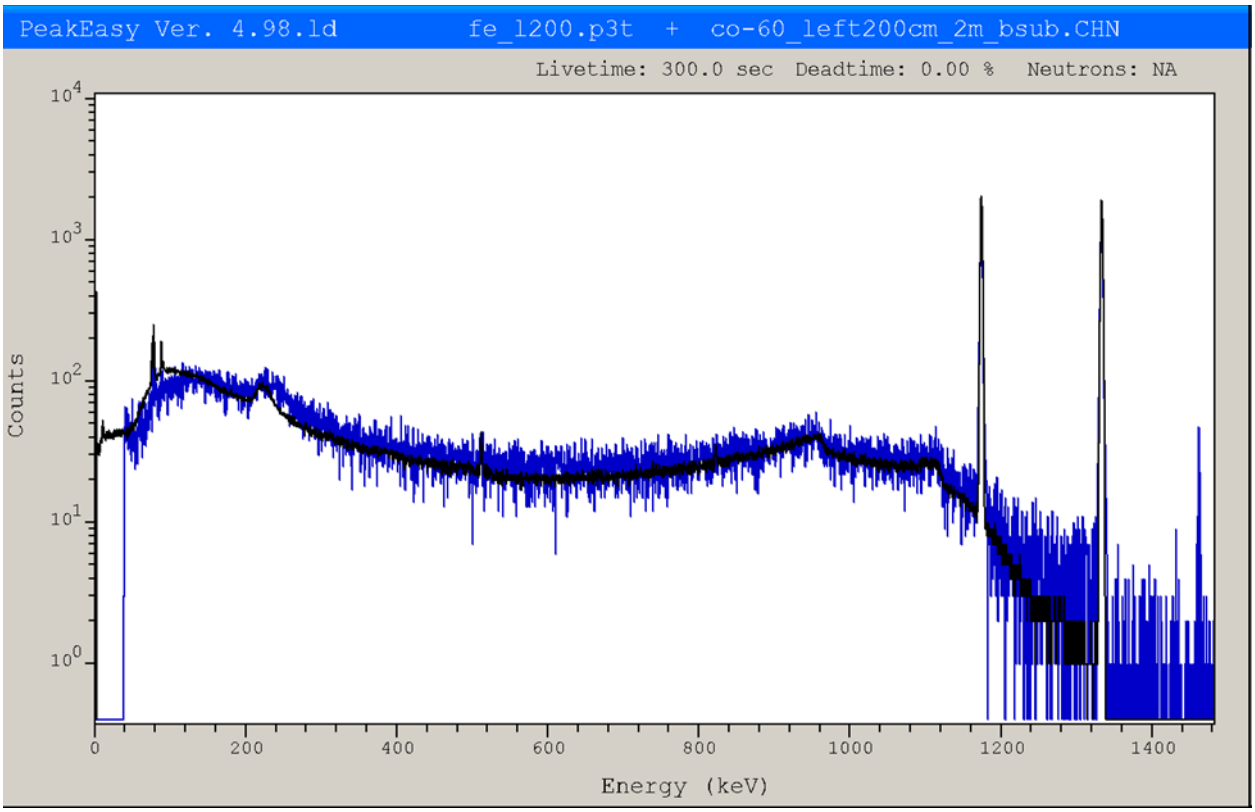

Figure 15. Spectra overlay, Left Offset 200 cm, Measured (Blue) vs Synthetic (Black)

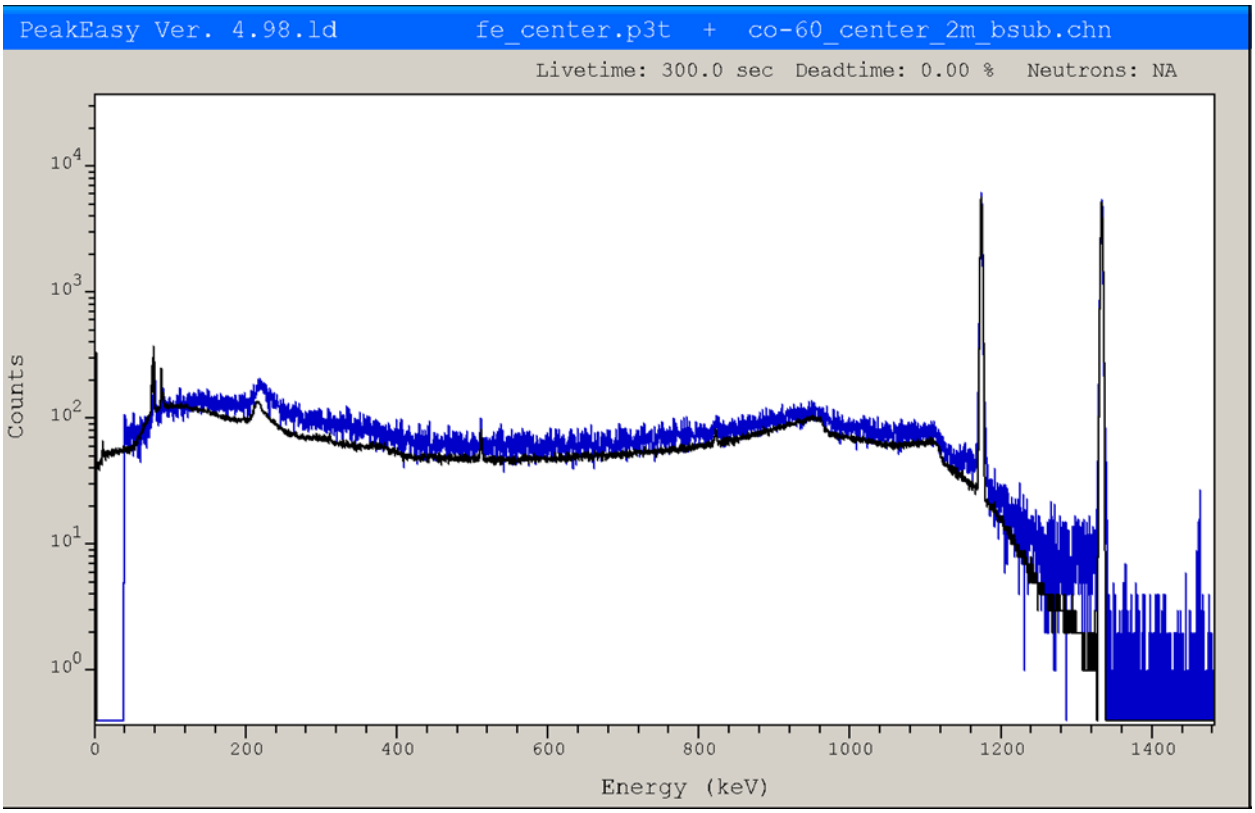

Figure 16. Spectra overlay, Center, Measured (Blue) vs Synthetic (Black)

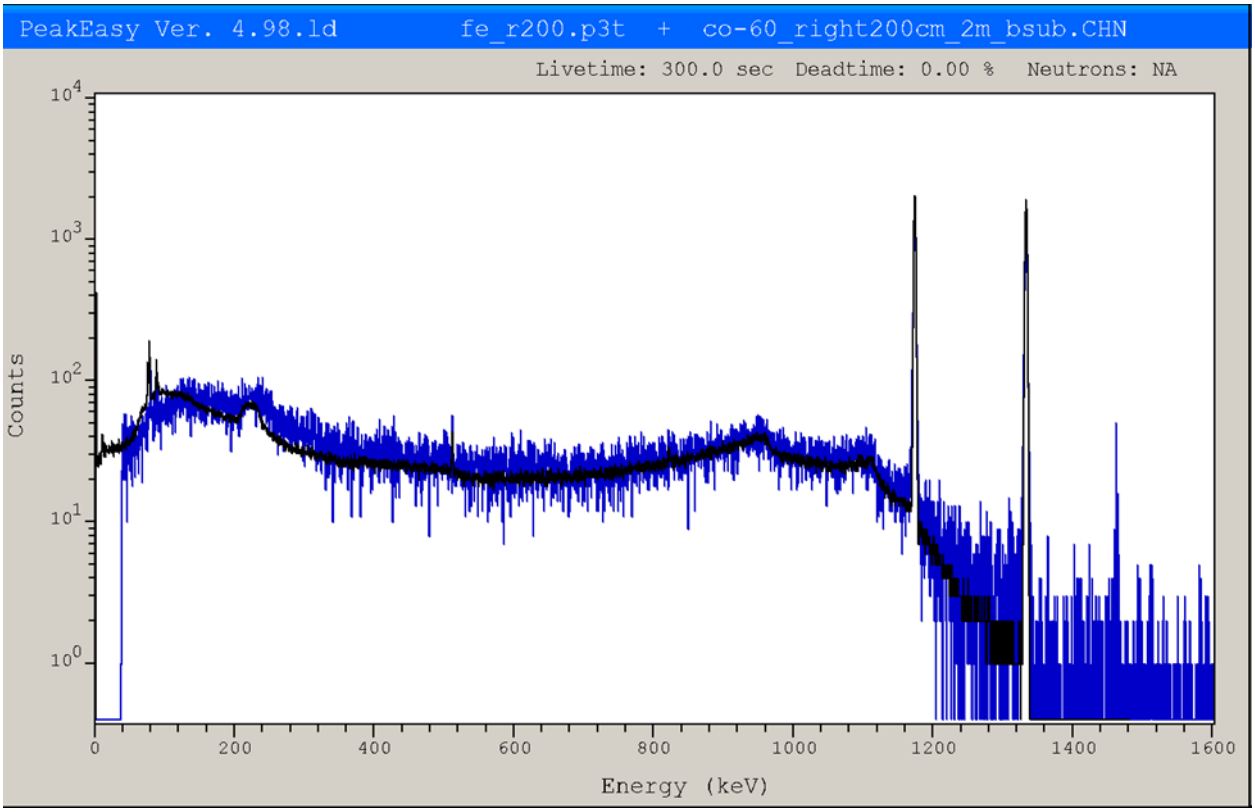

Figure 17. Spectra overlay, Right Offset 200 cm, Measured (Blue) vs Synthetic (Black)

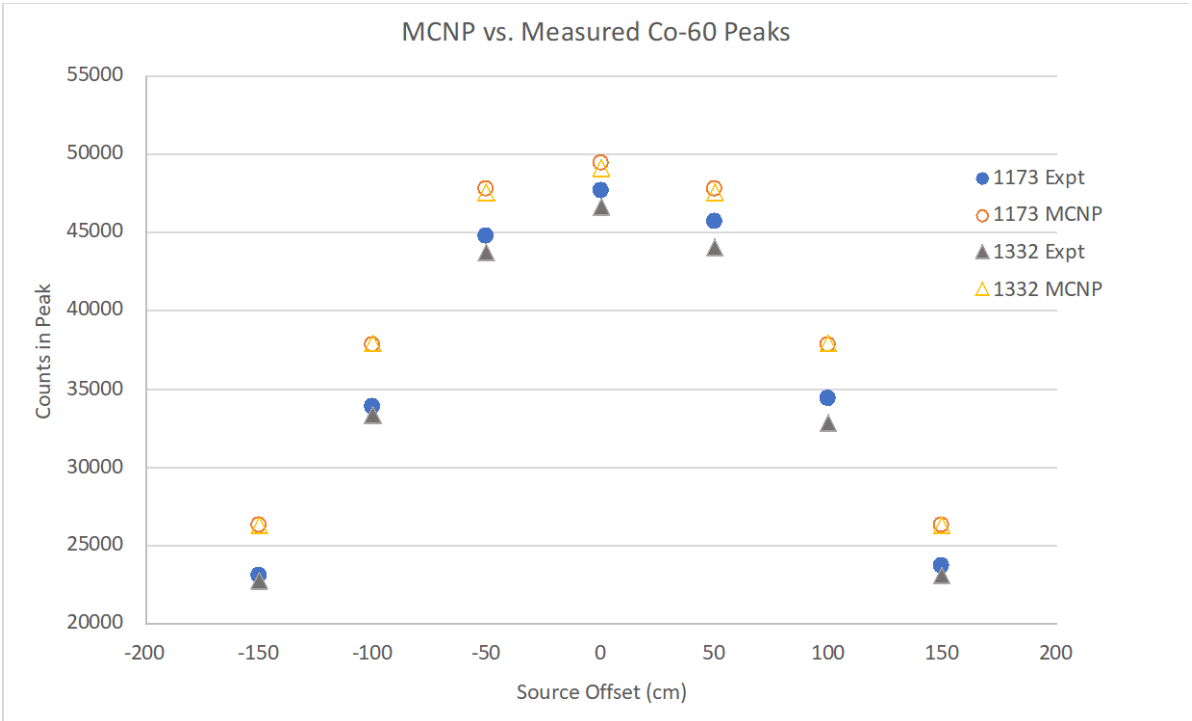

Figure 18. Plot of peak areas for 1173 and 1332 peaks from Co-60 as a function of offset (±200cm) at a 200cm distance.

4.3. Scatter

The iron box from the high areal density measurements was broken into its primary components: a front face or shield and a back face or backscatter element. Additionally, a large 4.9 mCi source was used in the shielded configuration. Table 4 shows the comparison between the measured and MCNP spectra, along with the box discussed previously for comparison. Figure 19-21 show the overlaid spectra. A prominent backscatter feature is visible in all spectra, but it is consistently over predicted by MCNP. For all cases, the peak area are in reasonable agreement. MCNP better predicts the continuum for the shielded case than the backscatter case, but both vary more from the measurement than the intact box for most criteria. There was more deviation from the measured spectrum for the big source than the smaller source.

Table 4. Quantitative Comparison between Measured and Synthetic Spectra- Scatter Measurements

Config	Absolute % Difference	Average % Difference	Chi Square	% More than 3 σ Difference	Gamma cps % Difference	% Difference, 1173 keV peak	% Difference, 1332 keV peak
Fe box from Set 1	12.4%	-6.4%	6.58	17.5%	-4.6%	2.4%	6.1%
Backscatter	21.7%	-20.8%	8.28	24.1%	-11.4%	5.6%	6.0%
Shielded	33.2%	-5.0%	5.27	14.1%	-7.3%	-8.4%	-1.7%
Big Source Shielded	18.6%	-13.5%	80.66	57.3%	-7.8%	6.9%	9.8%

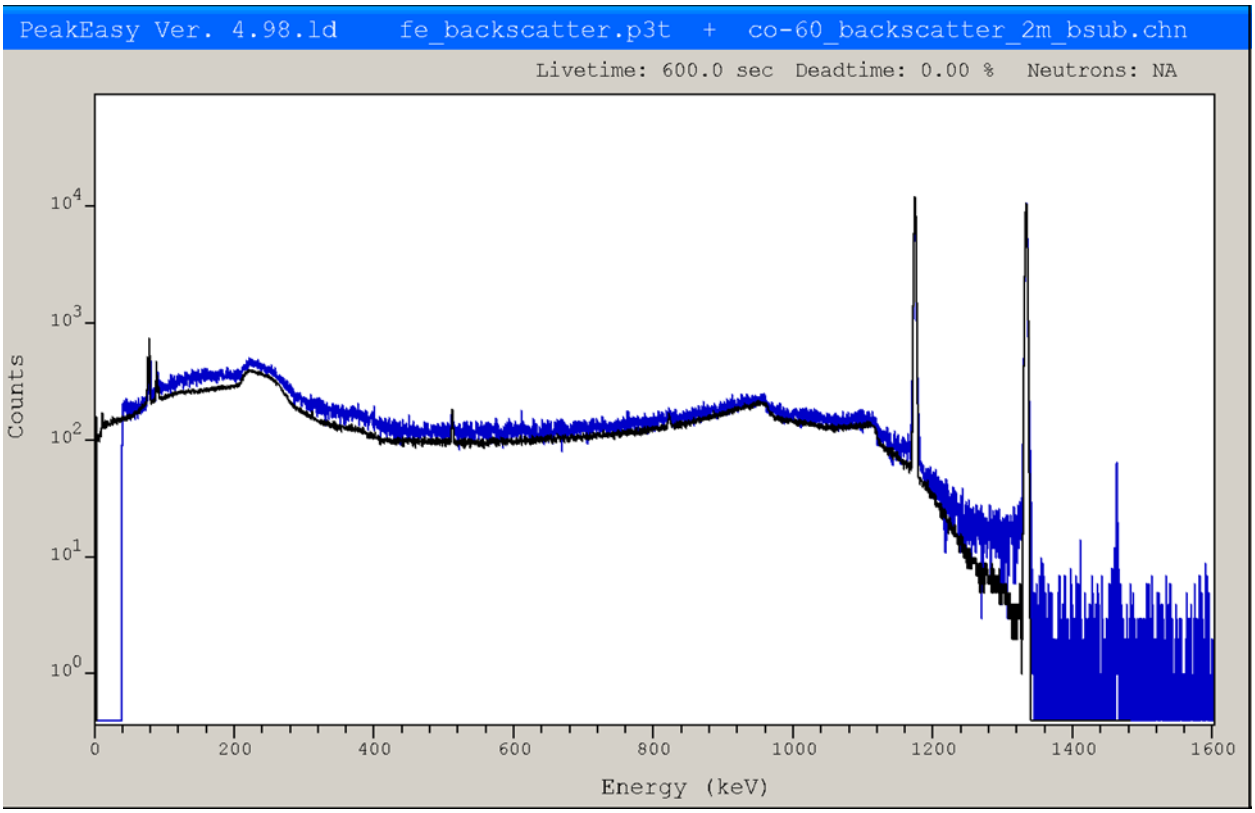

Figure 19. Spectra overlay, Backscatter, Measured (Blue) vs Synthetic (Black)

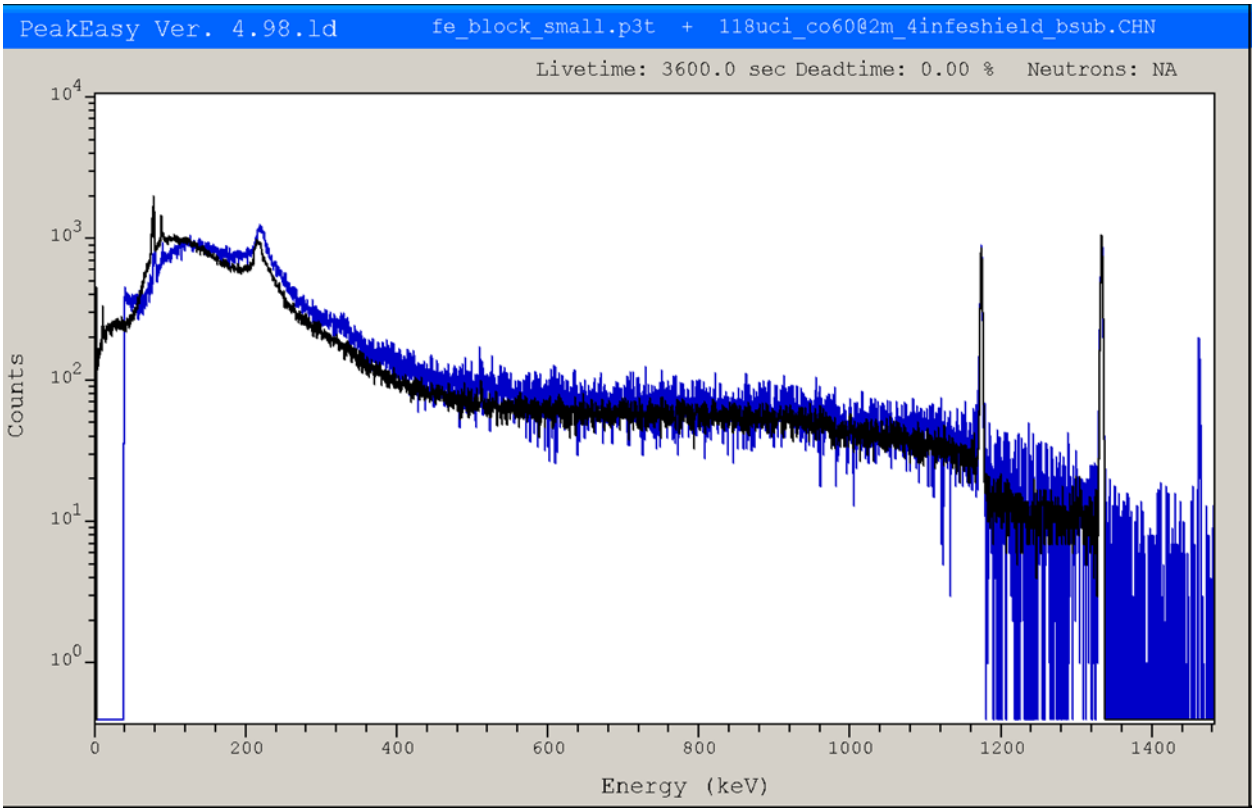

Figure 20. Spectra overlay, Shielded, Measured (Blue) vs Synthetic (Black)

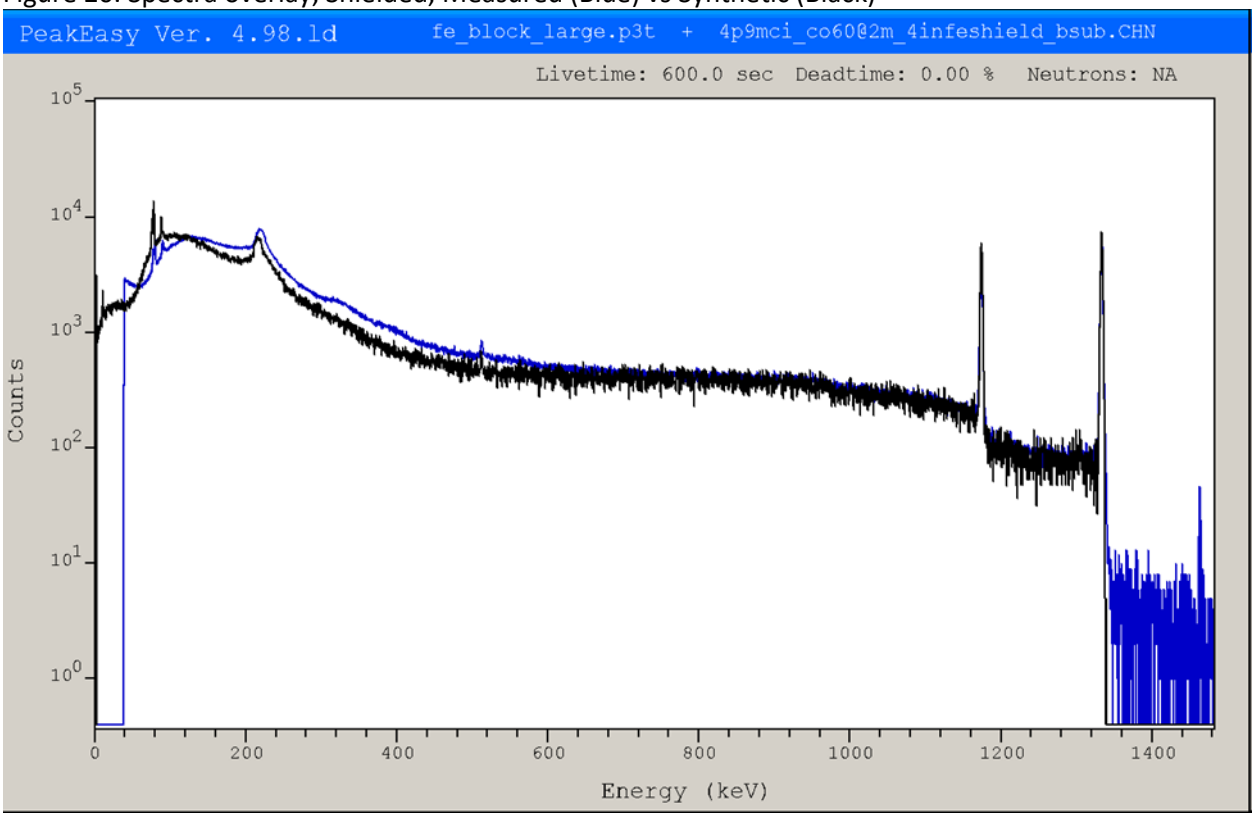

Figure 21. Spectra overlay, Big Source Shielded, Measured (Blue) vs Synthetic (Black)

4.4. Order of Shielding

Varying the order for multiple shielding materials does impact the synthetic spectra's match to measured spectra. In these cases, the results from MCNP match the experiments generally well. Table 5 shows the quantitative comparisons, and Figures 22 and 23 show the spectrum overlays. In the case where the iron is inside of the polyethylene, the match is closer to the experimental measurement in most metrics. However, there is a poor fit in the low energy region. For the case with polyethylene inside of the iron MCNP predicts peaks that are too large and over-predicts the continuum. This suggests the MCNP physics is weaker when transporting gammas through a hydrogenous material than the previous configuration examined.

Table 5: Quantitative Comparison between Measured and Synthetic Spectra- Order of Shielding Measurements

Config	Absolute % Difference	Average % Difference	Chi Square	% More than 3 σ Difference	Gamma cps % Difference	% Difference, 1173 keV peak	% Difference, 1332 keV peak
FePE	22.3%	-10.0%	2.66	4.6%	-10.0%	-4.6%	-3.2%
PEFe	25.8%	17.8%	2.80	2.6%	10.0%	31.1%	26.1%

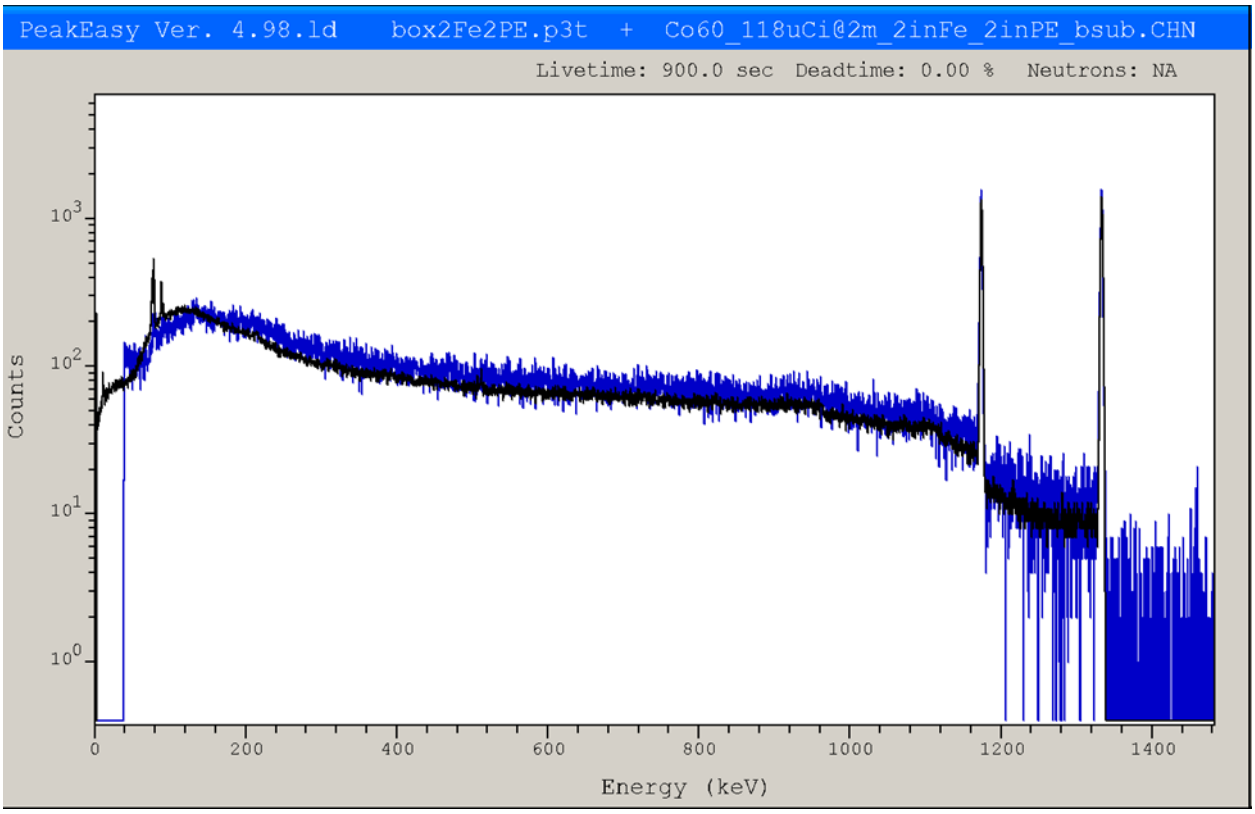

Figure 22. Spectra overlay, Iron-Polyethylene, Measured (Blue) vs Synthetic (Black)

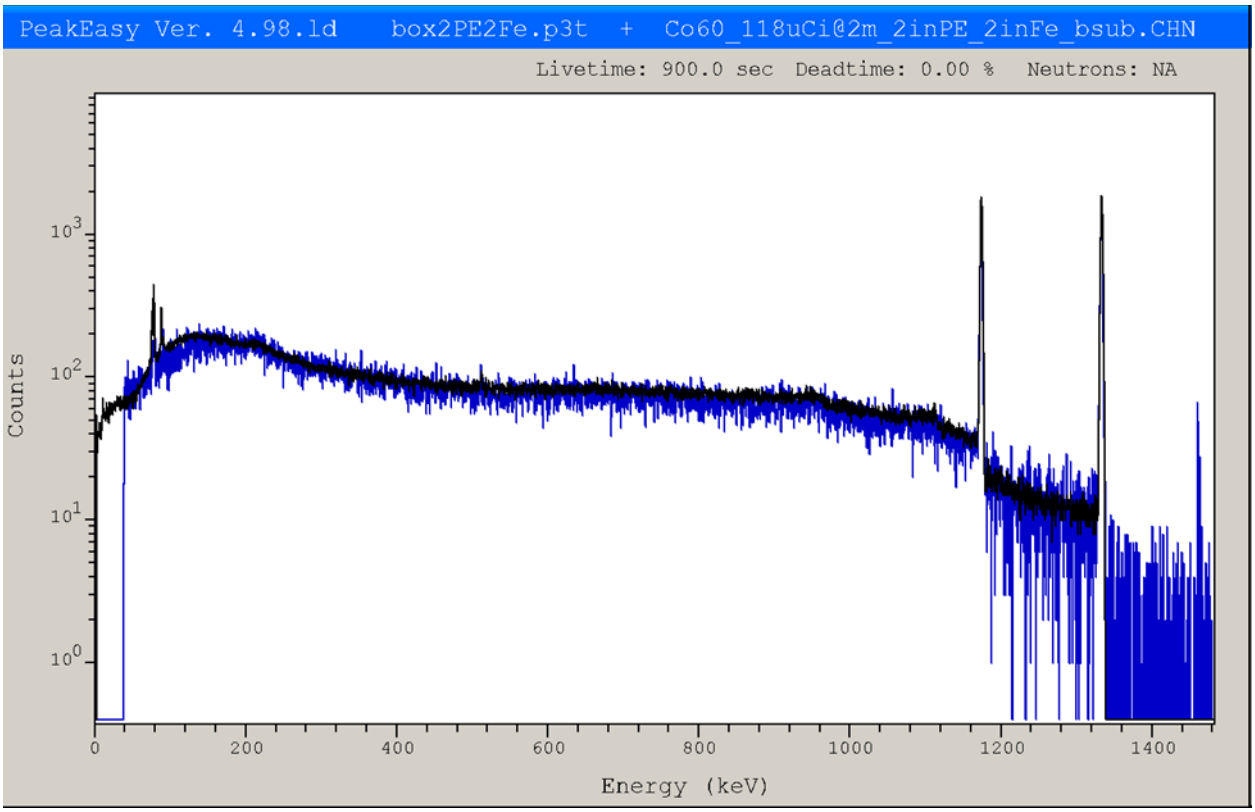

Figure 23. Spectra overlay, Polyethylene-Iron, Measured (Blue) vs Synthetic (Black)

4.5. Increasing Shielding Thickness

For this set of configurations, a bare Co-60 or Cf-252 source was placed inside increasingly thick polyethylene shielding: 2.5”, 3.5” and 4.5”. The results from the Co-60 source are shown in Table 6 and Figures 24-27. The shielded cases were very similar to the unshielded case, with additional shielding actually matching the experimental spectra slightly better than the bare unshielded source across all metrics. Again, MCNP under-predicts both peak area and the continuum, but peak areas are generally in good agreement.

Table 6. Quantitative Comparison between Measured and Synthetic Spectra- Increasing Polyethylene Shielding with Co-60 Measurements

Config	Absolute % Difference	Average % Difference	Chi Square	% More than 3 σ Difference	Gamma cps % Difference	% Difference, 1173 keV peak	% Difference, 1332 keV peak
Co-60_unshielded	28.3%	-26.7%	12.15	43.9%	-18.0%	-6.8%	-1.7%
Co-60_2.5"PE	22.9%	-20.8%	8.40	28.5%	-14.1%	-6.6%	-1.9%
Co-60_3.5"PE	22.3%	-19.5%	8.14	27.3%	-12.7%	-5.9%	-0.7%
Co-60_4.5"PE	21.1%	-17.6%	7.52	22.0%	-10.6%	-7.0%	-1.7%

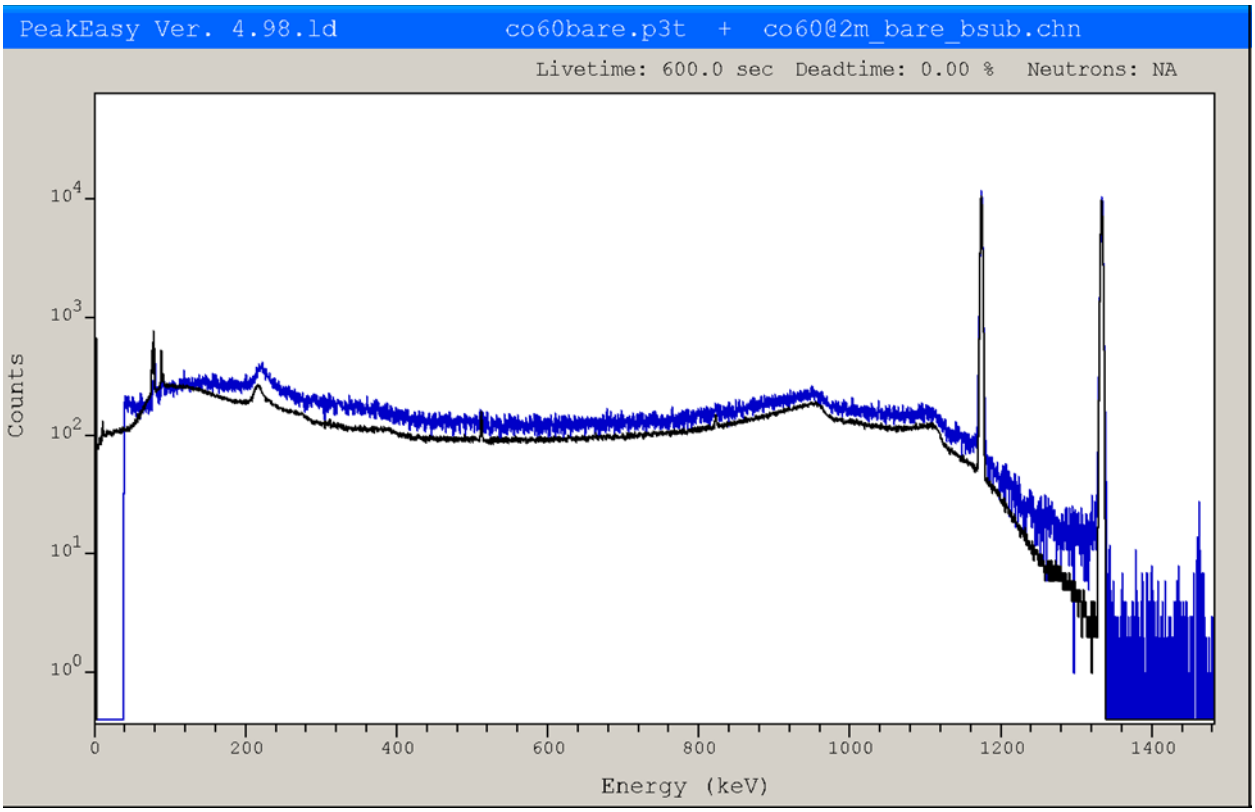

Figure 24. Spectra overlay, Co-60 unshielded, Measured (Blue) vs Synthetic (Black)

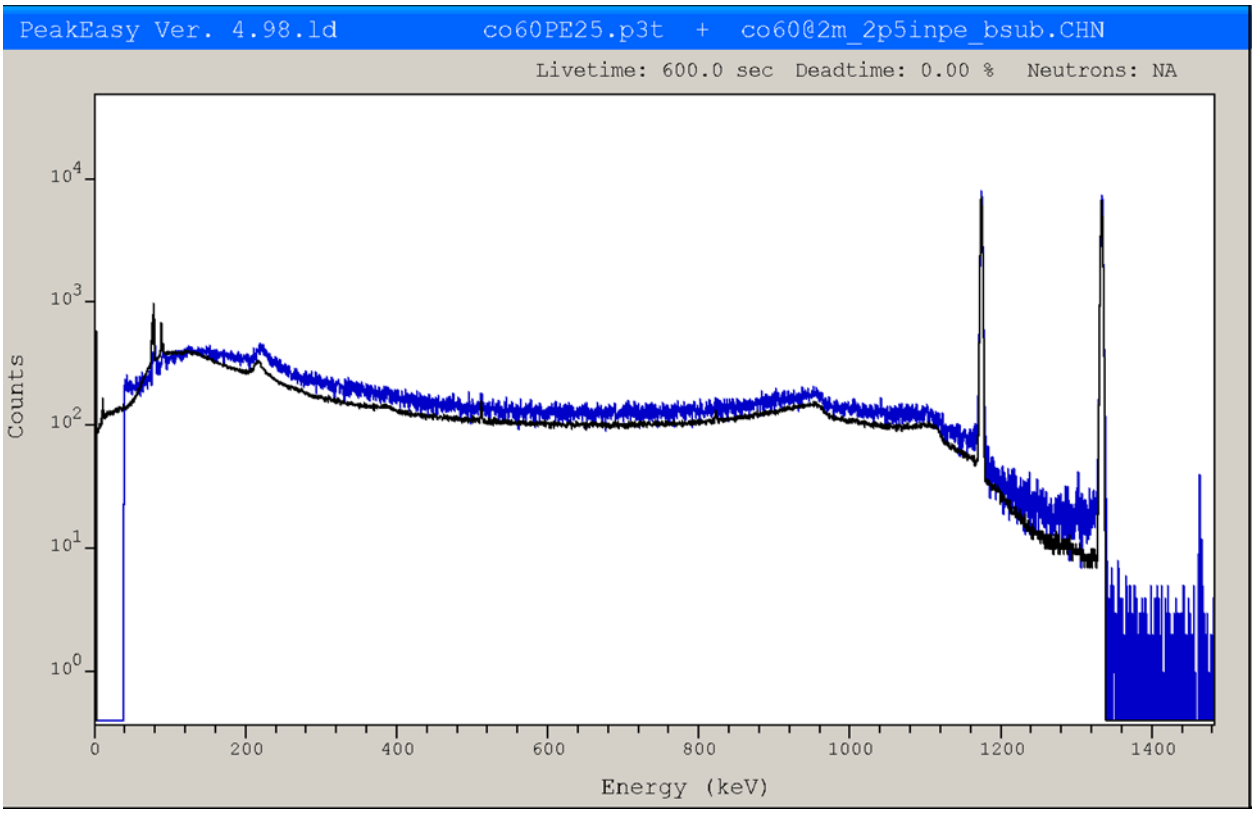

Figure 25. Spectra overlay, Co-60 in 2.5” Polyethylene, Measured (Blue) vs Synthetic (Black)

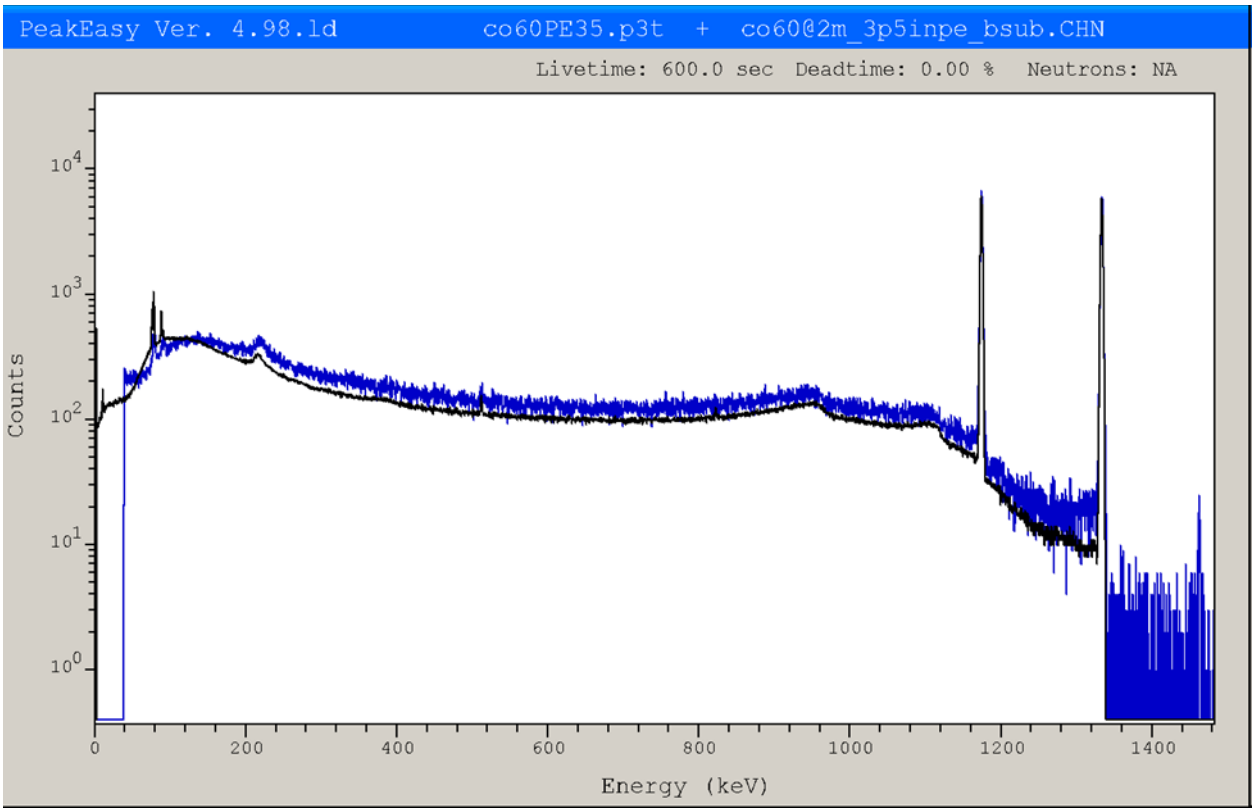

Figure 26. Spectra overlay, Co-60 in 3.5” Polyethylene, Measured (Blue) vs Synthetic (Black)

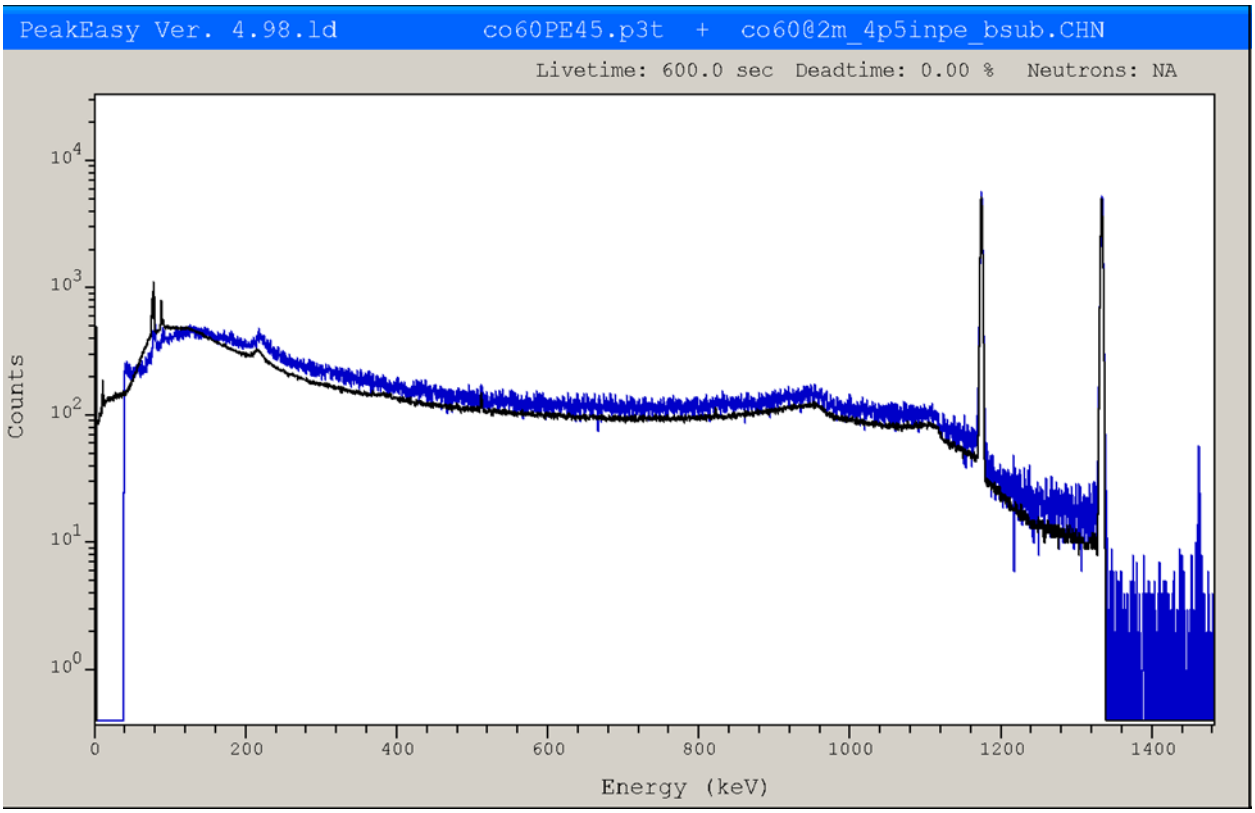

Figure 27. Spectra overlay, Co-60 in 4.5” Polyethylene, Measured (Blue) vs Synthetic (Black)

The Cf-252 cases required using a more complicated source in MCNP: a spectrum of gamma rays generated by the GADRAS source model was used in conjunction with a Watt spectrum neutron source. The 57.1 μCi Cf-252 source was modeled with the two particle types weighted such that there were 0.317 neutrons and 0.683 gammas per source particle. The tallies were then normalized to the source activity and count length. The comparisons between the measured spectra and the MCNP results are shown in Table 7 and Figures 28-31. Evaluating the results are more challenging than the Co-60 spectra which possess only two photopeaks. The Cf-252 spectrum is complicated with many minor peaks from contaminants, fission products, and neutron-induced gamma-rays. It is expected that these will not be predicted well, so the continuum will be a worse fit generally than the Co-60. A primary peak for the Cf-252 in polyethylene is the hydrogen capture line at 2223 keV. This was used as a marker for the prediction of interactions. With the bare source, MCNP significantly under-predicted hydrogen capture. However, with the polyethylene shield, the predicted 2223 keV matched well to the measured spectrum.

Table 7. Quantitative Comparison between Measured and Synthetic Spectra- Increasing Polyethylene Shielding with Cf-252 Measurements

Config	Absolute % Difference	Average % Difference	Chi Square	% More than 3 σ Difference	Gamma cps % Difference	% Difference, 2223 keV peak
Cf-252_ unshielded	54.3%	36.5%	8.71	6.1%	2.0%	-61.6%
Cf-252_2.5"PE	50.0%	-25.9%	6.06	22.2%	-43.6%	-5.4%
Cf-252_3.5"PE	53.1%	-18.5%	5.13	19.5%	-41.1%	-0.5%
Cf-252_4.5"PE	52.5%	-16.2%	3.87	13.5%	-36.9%	5.1%

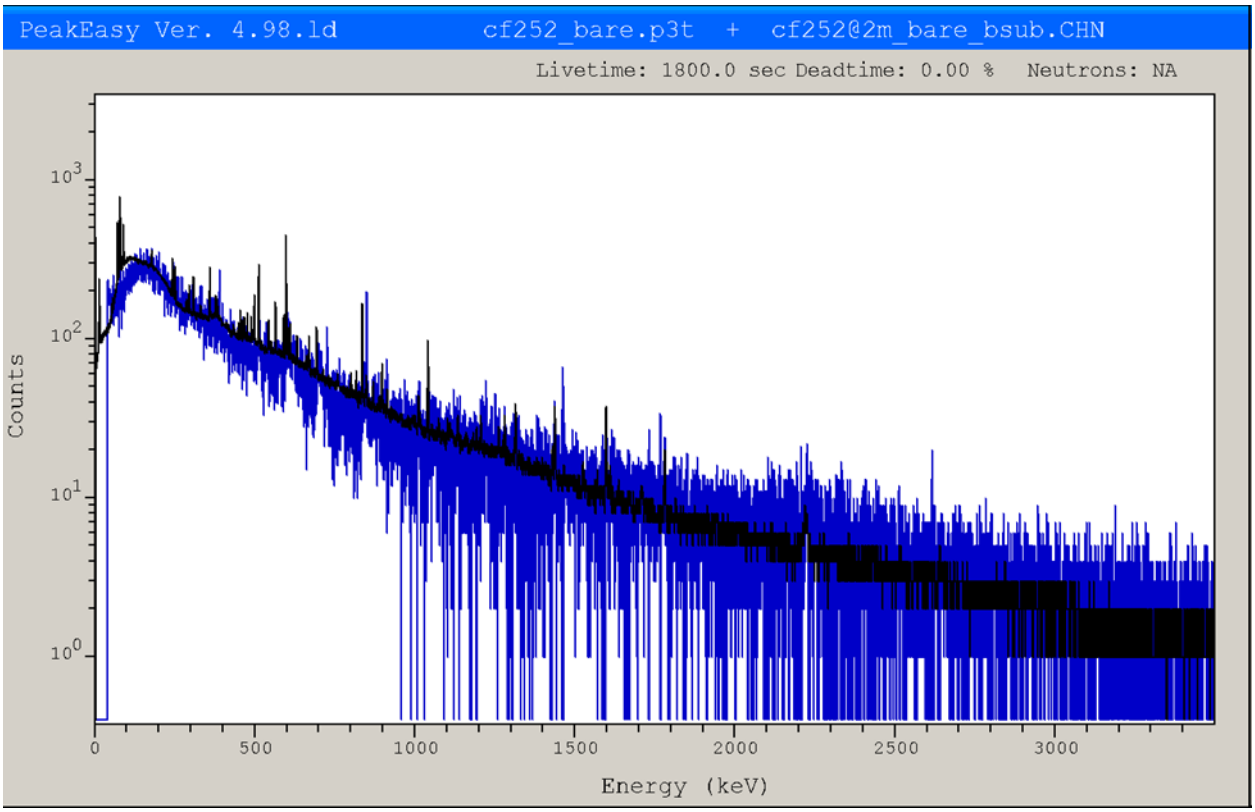

Figure 28. Spectra overlay, Cf-252 unshielded, Measured (Blue) vs Synthetic (Black)

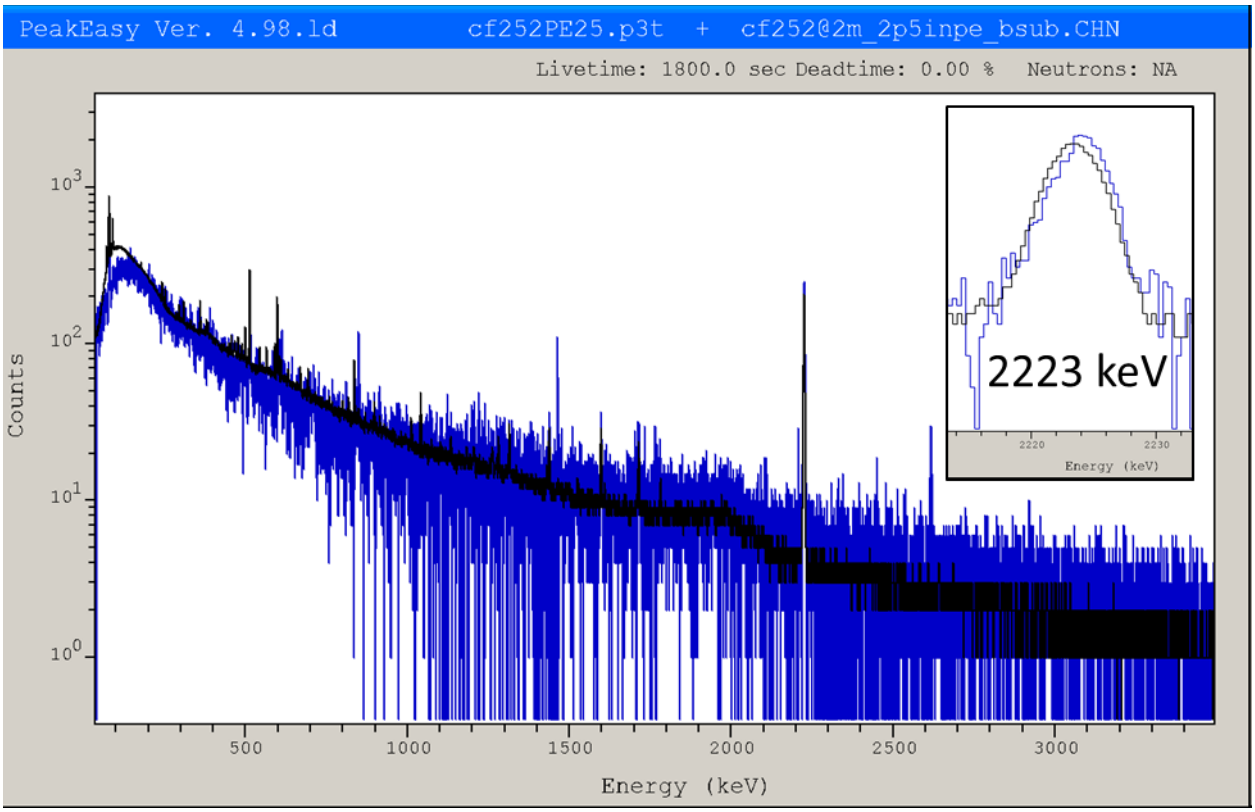

Figure 29. Spectra overlay, Cf-252 in 2.5" Polyethylene, Measured (Blue) vs Synthetic (Black)

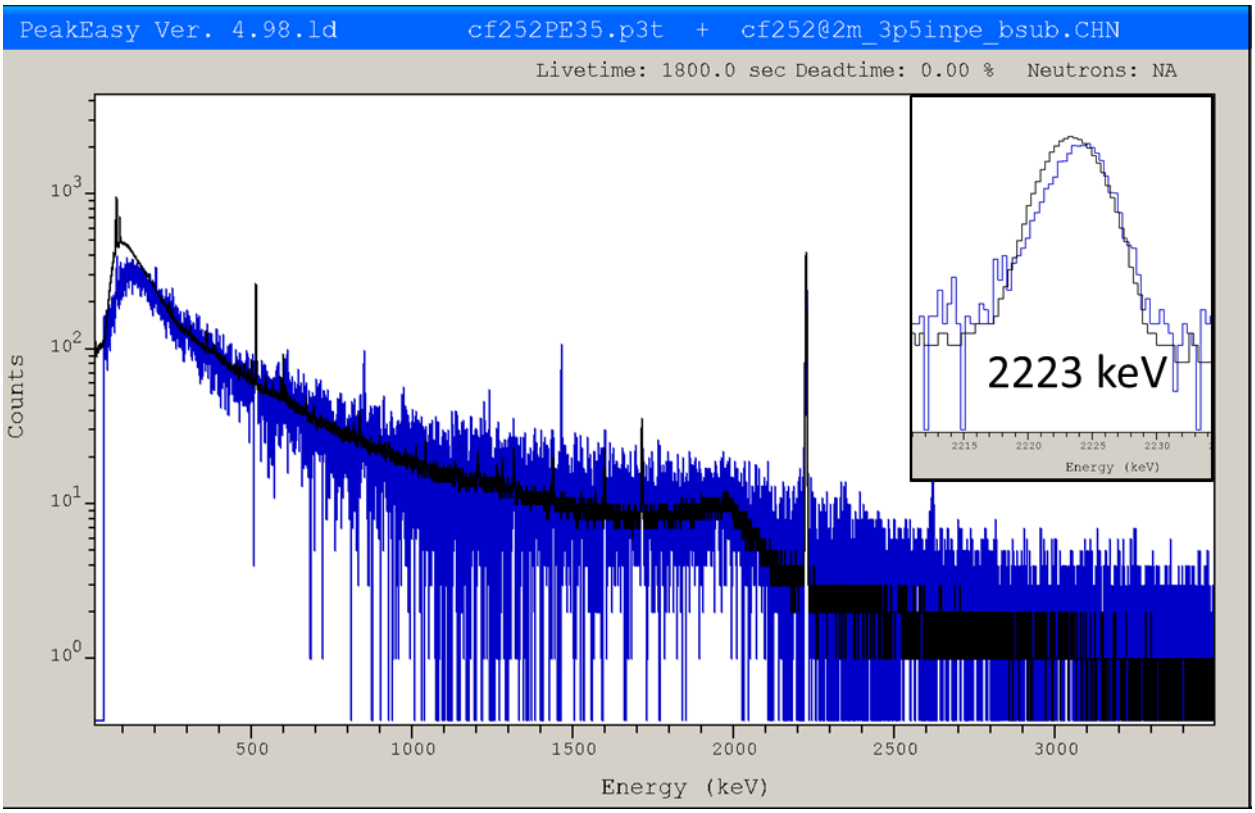

Figure 30. Spectra overlay, Cf-252 in 3.5" Polyethylene, Measured (Blue) vs Synthetic (Black)

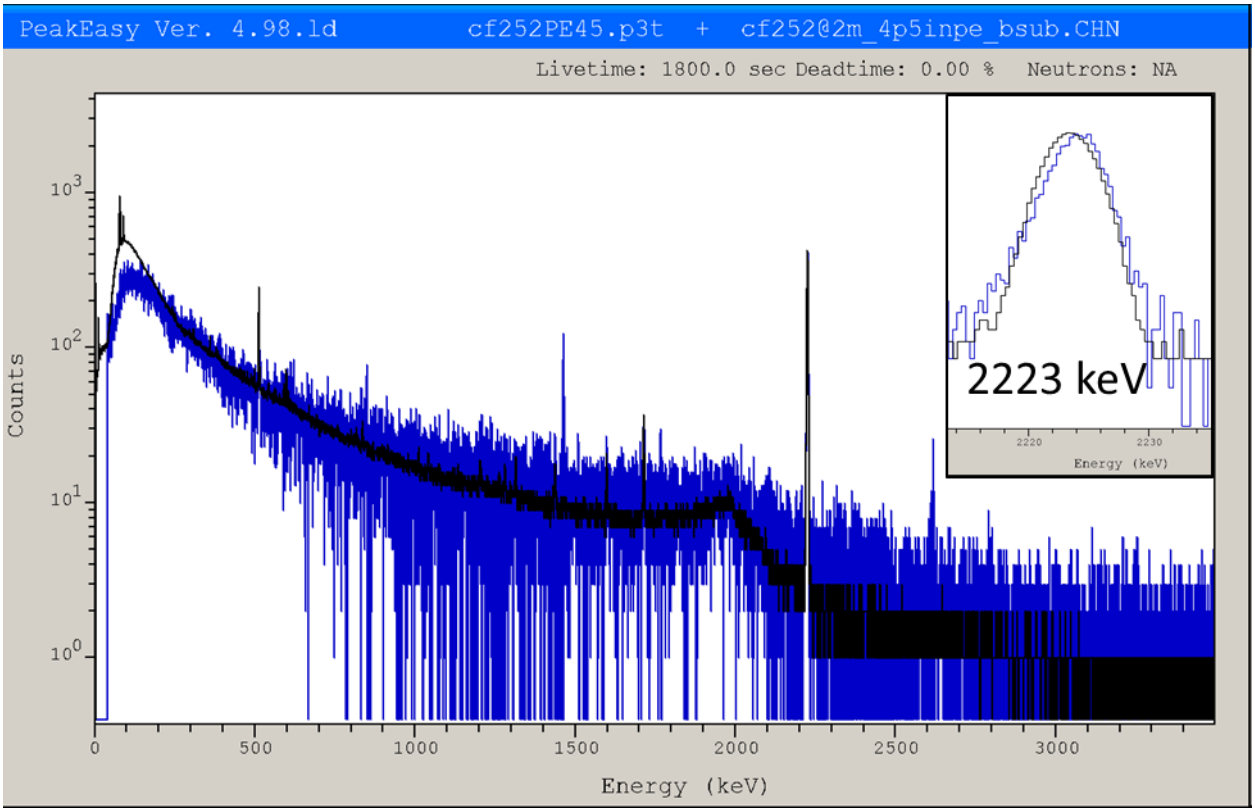

Figure 31. Spectra overlay, Cf-252 in 4.5" Polyethylene, Measured (Blue) vs Synthetic (Black)

4.6. DU Shells

In the case of the DU shells, the source used was taken from the GADRAS source model, which outputs an MCNP-structured source. This source is very slow and awkward to run in practice, so an intermediate MCNP run was made to tally the exterior leakage from the GADRAS-generated volume source. This leakage was tallied using a detailed energy bin structure in order to distinguish gamma peaks from the continuum background. Unfortunately, this source did not converge well and had considerable noise. A 5 channel smoothing was applied to reduce this but the resultant source, when put back into an MCNP geometry, still has numerous artificial lines in the spectrum output from the detector tally. Although the continuum match to the measured data is consistent with some other cases, there is more than a 30% difference in 186 keV and 1001 keV peak areas and numerous peak-like artifacts.

Table 8. Quantitative Comparison between Measured and Synthetic Spectra- Increasing Thickness with DU Shells

Config	Absolute % Difference	Average % Difference	Chi Square	% More than 3 σ Difference	Gamma cps % Difference	% Difference, 186 keV peak	% Difference, 1001 keV peak
DU-4 in	38.6%	20.6%	6.16	10.7%	15.8%	36.5%	33.9%

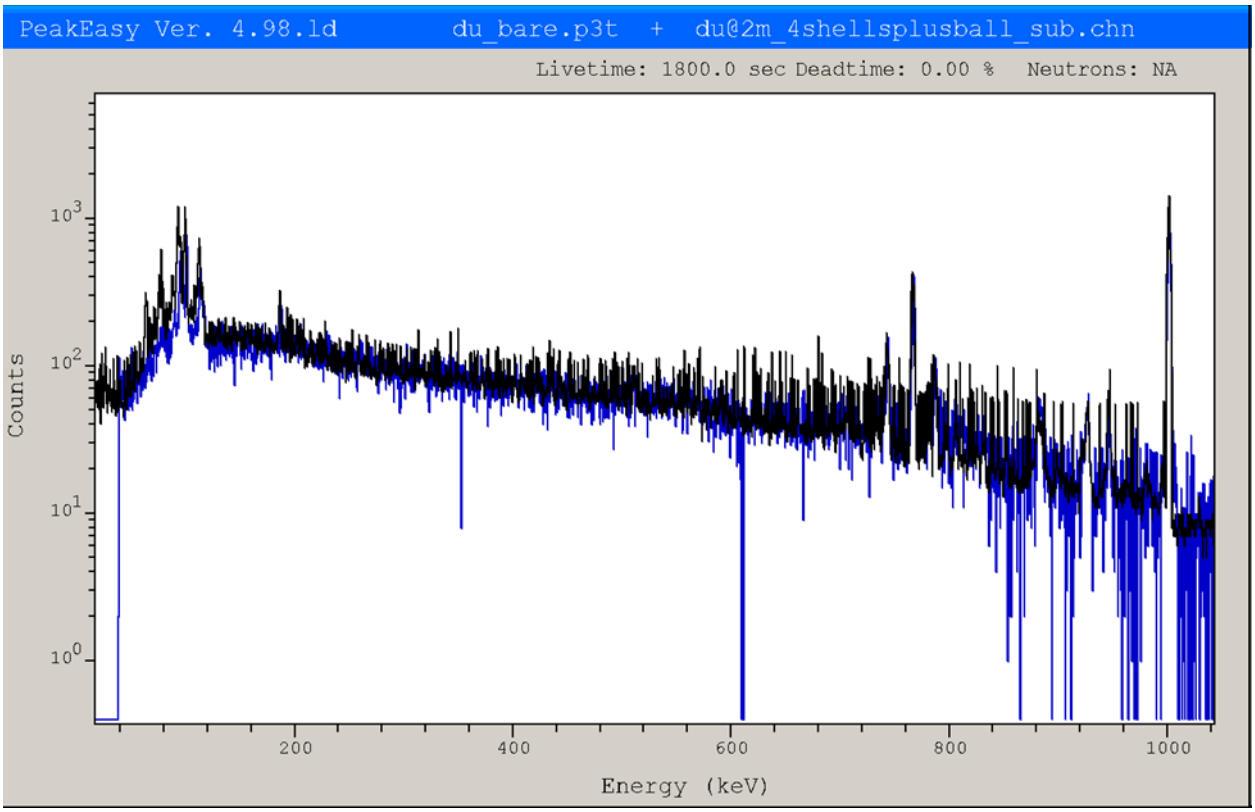

Figure 32. Spectra overlay, DU- 4" sphere, Measured (Blue) vs Synthetic (Black)

4.7. With and Without Bi Side Shield

MCNP spectra were qualitatively compared to a series of measurements with the Bi side shield removed. This was done to explore the effect of the side shield as a potential factor in the unexpected deviation between simulation and experiment for translated sources. A new response function was not generated, so qualitative comparisons were not done. Figures 33 and 34 show the comparisons for the source at 90° from the detector, where the gamma rays are not striking the face of the detector, rather the source is directly side-on to the detector, with and without the side shield. The peaks are in good agreement for both measurements, and at least some of the poor continuum fit without the Bi can be attributed to the difference in modeling versus measurement from the response function.

The second set of measurements conducted without the side shield was a repeat of the previously reported Offset configurations. Figures 35, 36, and 37 show overlays of the left-most, center, and right-most cases. The peak areas are consistent, but again, the continuum is poorly predicted in low and moderate energy ranges. This can be attributed in part to the use of the response function for the detector with the bismuth side shield when modeling the unshielded spectra and discrepancies in transport through the side shield at angles.

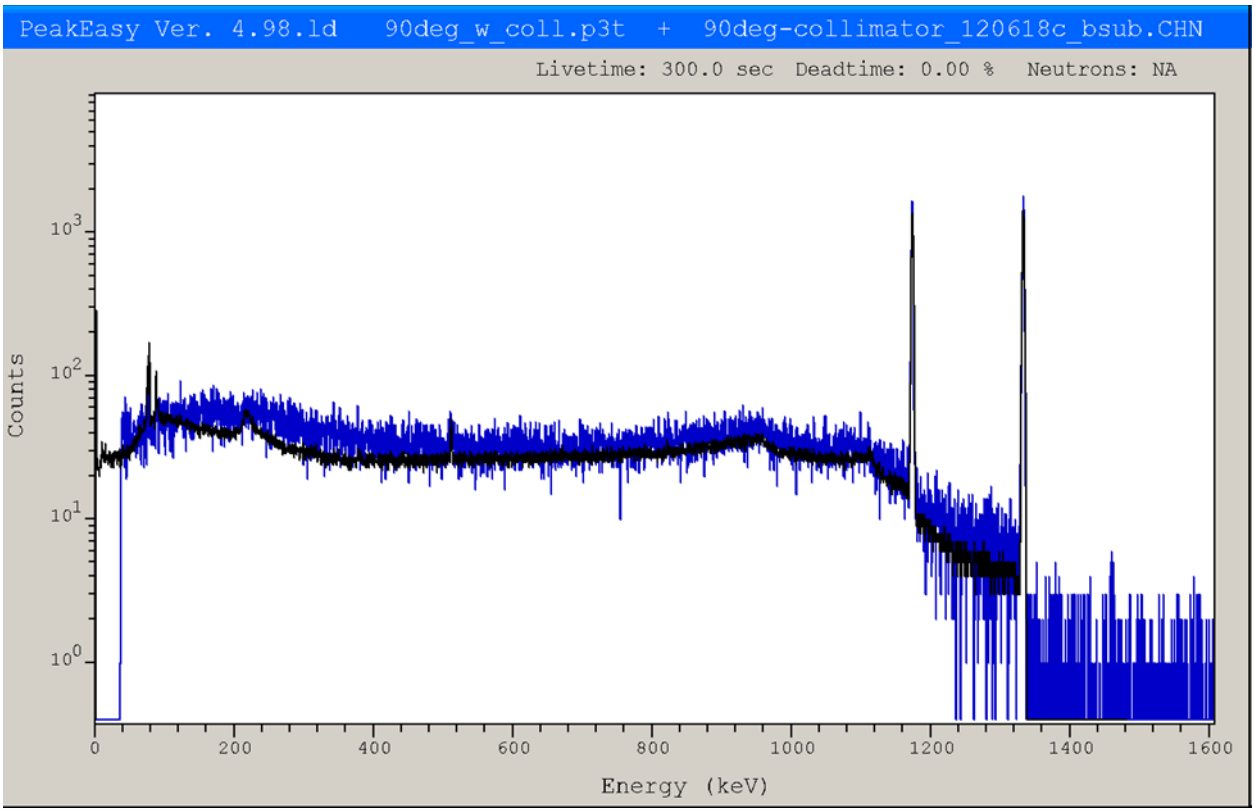

Figure 33. Spectra overlay, Source at 90° with Bi side shield, Measured (Blue) vs Synthetic (Black)

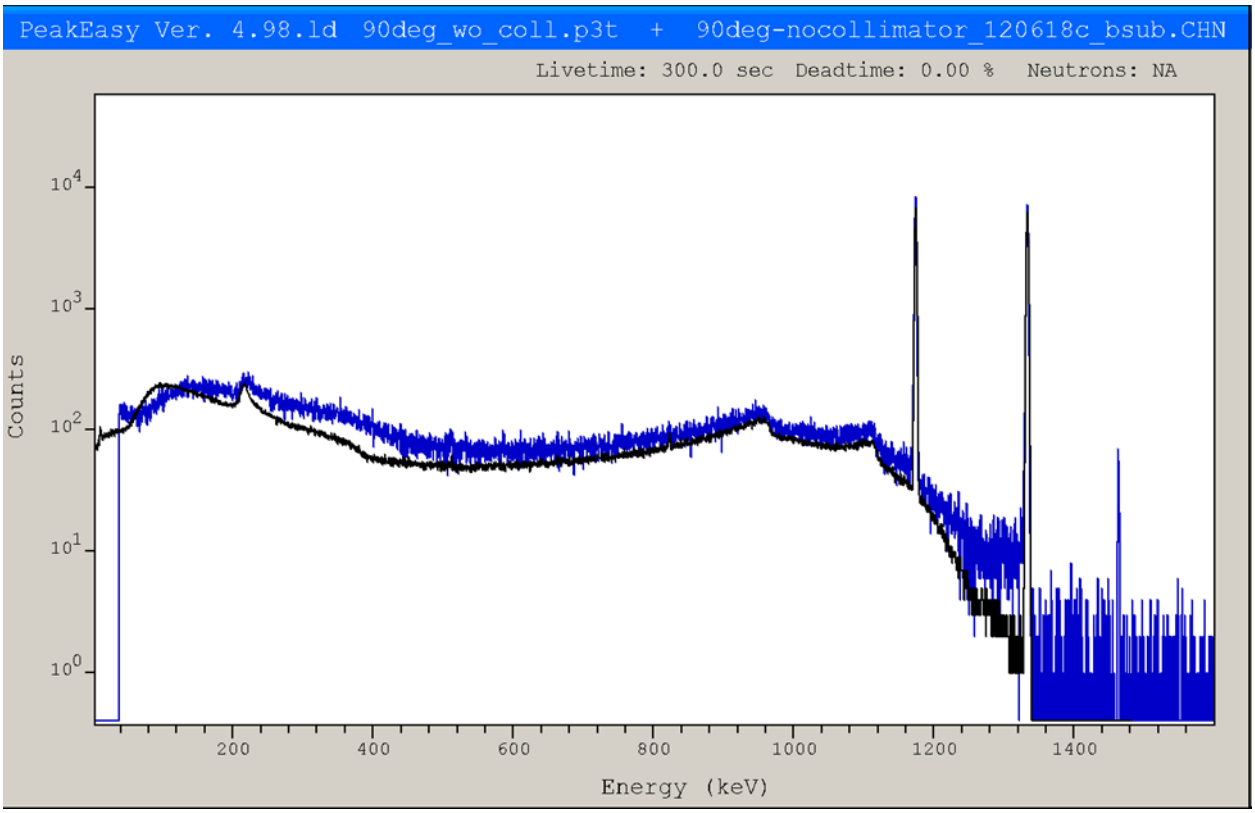

Figure 34. Spectra overlay, Source at 90° without Bi side shield, Measured (Blue) vs Synthetic (Black)

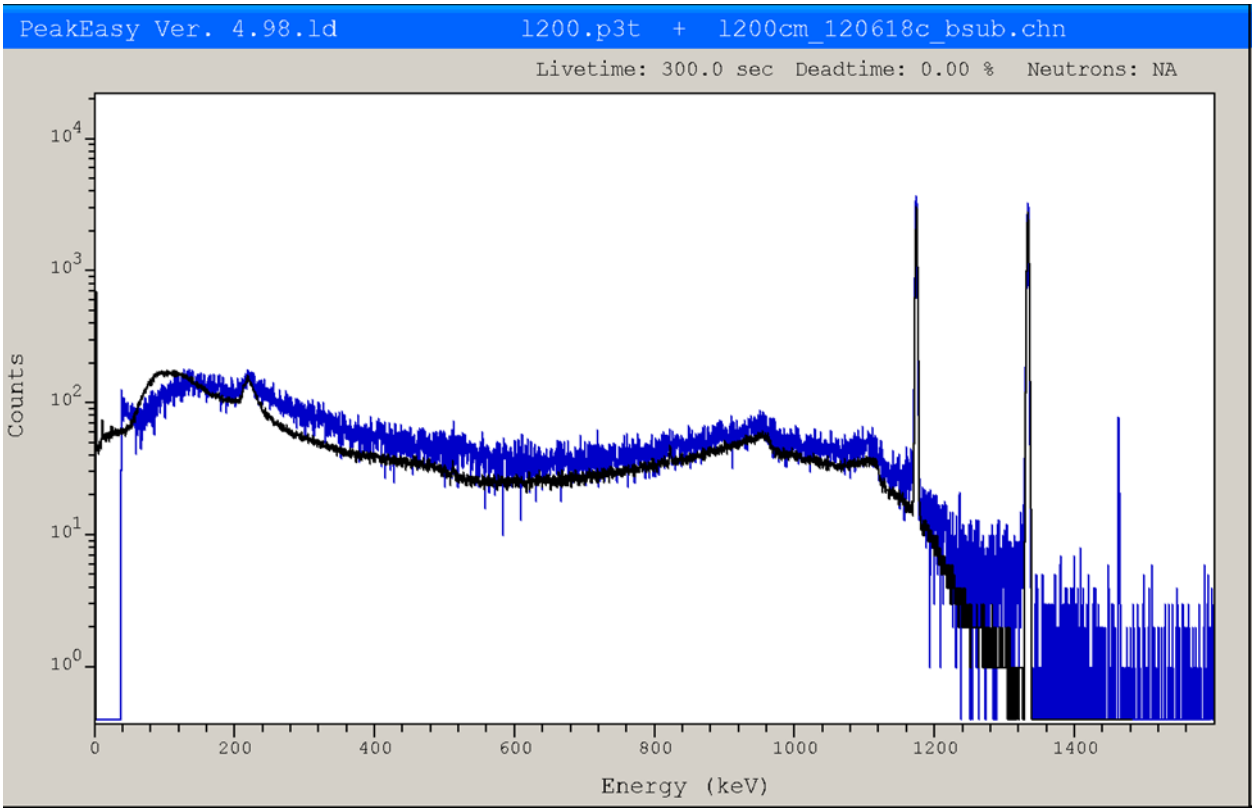

Figure 35. Spectra overlay, Left Offset 200 cm, Measured (Blue) vs Synthetic (Black)

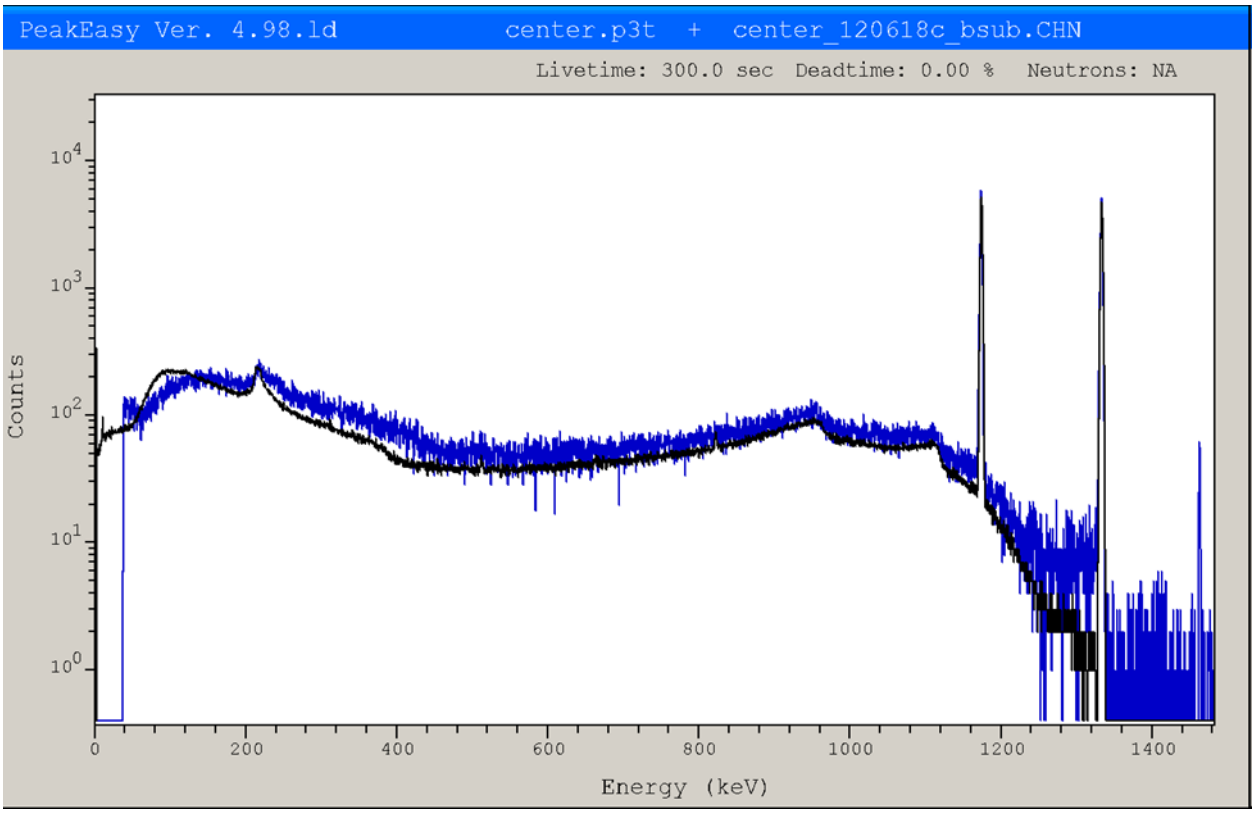

Figure 36. Spectra overlay, Center, Measured (Blue) vs Synthetic (Black)

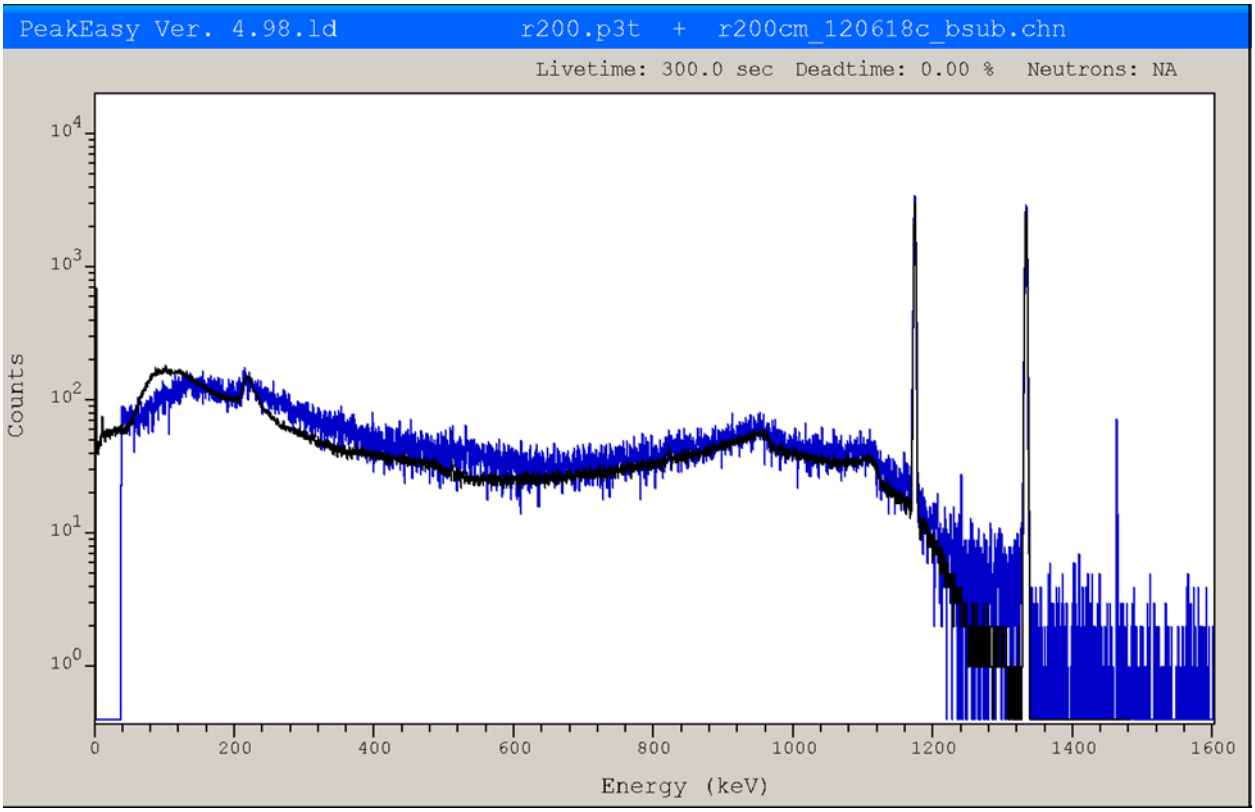

Figure 37. Spectra overlay, Right Offset 200 cm, Measured (Blue) vs Synthetic (Black)

4.8. Discussion

MCNP is widely used to generate synthetic spectra that are increasingly relied on in lieu of measured data. To evaluate how well the modeled spectra match measured data, a series of simple measurements were conducted, primarily with Co-60, which has only two distinct photopeaks. Most configurations did reasonably well matching the full energy photopeaks. Configurations containing both metal and hydrogenous shielding (lead and MHE, iron and polyethylene) had poorer peak fits than configurations with only metal or only hydrogenous shielding. This seems to suggest some weakness in the physics or data in MCNP with respect to multiple layers. Additionally, at a 45° angle to the detector, the photopeak fits were becoming unacceptable. This is of particular relevance with respect to using synthetic data to evaluate portals or mobile systems where off-angle measurements are a critical component to detection.

Table 9, below, shows whether the synthetic spectrum over- or under-predicts counts in the region based on the average percent difference (positive or negative) and the percentage of channels in that band greater than 3 sigma from measured. With one exception, the MCNP model underpredicts the continuum in both the 200-400 keV and 400-1100 keV regions. In the lowest energy range, the results were mixed: relatively simple configurations like the offset configurations nearest the center and most single material shields followed that trend of under predicting the continuum. However, layered shielding materials and offsets where the majority of the gamma rays passed through the Bi side shield before reaching the detector consistently over predicted in the low energy region. This may indicate a

limitation in transfer between shielding materials in the calculations. Additionally, the germanium dead layer is not well known, and gamma rays at very low energy are sensitive to changes in this unknown layer. However, if this were the dominating factor, we would expect a similar trend in over-or under predicting at very low energies, which is not the case.

Table 9. Goodness-of-fit in Energy Bands, Percent of Channels More than 3 Sigma from Measured

	Full Energy Range	40-200 keV	200-400 keV	400-1100 keV
Fe Box	↓ 17.5%	↑ 34.5%	↓ 48.7%	↓ 8.0%
Pb Box	↓ 52.2%	↓ 35.6%	↓ 77.7%	↓ 59.1%
Pb Sphere	↓ 59.7%	↓ 59.9%	↓ 96.9%	↓ 62.3%
Pb-MHE Sphere	↓ 93.4%	↑ 76.4%	↓ 99.8%	↓ 99.7%
L-200	↓ 3.2%	↑ 11.9%	↓ 2.0%	↓ 0.2%
L-150	↓ 3.6%	↑ 8.1%	↓ 6.1%	↓ 0.4%
L-100	↓ 4.7%	↑ 7.6%	↓ 9.5%	↓ 1.0%
L-50	↓ 7.2%	↓ 7.8%	↓ 18.7%	↓ 2.7%
Center	↓ 12.9%	↓ 12.1%	↓ 34.3%	↓ 6.5%
R-50	↓ 8.8%	↓ 9.4%	↓ 21.2%	↓ 3.9%
R-100	↓ 5.0%	- 6.7%	↓ 11.3%	↓ 1.4%
R-150	↓ 4.2%	↑ 6.7%	↓ 10.8%	↓ 0.4%
R-200	↓ 3.0%	↑ 6.7%	↓ 4.3%	↓ 0.3%
Backscatter	↓ 24.1%	↓ 64.5%	↓ 47.4%	↓ 9.6%
Shielded	↓ 14.1%	↑ 51.5%	↓ 38.6%	↓ 2.6%
Big Shielded	↓ 57.3%	- 92.1%	↓ 100.0%	↓ 48.6%
FePE	↓ 4.6%	↑ 9.2%	↓ 8.4%	↓ 2.6%
PEFe	↑ 2.6%	↑ 6.3%	↑ 0.7%	↑ 1.5%

The Cf-252 and DU present challenges to modeling in MCNP. While the Co-60 source term was straightforward, generating source terms for the neutron source and the depleted uranium were not. The majority of the gamma rays in the Cf-252 spectrum are not from the Cf-252 itself, rather they are from neutron interactions with the environment. This makes them particularly difficult to predict. MCNP did reasonably well with the hydrogen n-gamma when there was hydrogenous shielding but under predicted it bare, probably due to interactions in the environment that were not accounted for in the model. The DU fit was quite poor due to challenges generating the source term and getting to convergence.

5. Comparison between GADRAS and MCNP Results

A critical question when generating synthetic spectra to use in evaluating detectors is: is it good enough? Then if it isn't good enough, are there other methods or techniques that can generate spectra that are good enough? GADRAS can be used to generate a large amount of synthetic data in a relatively short amount of time, but it uses some approximations in its calculations. MCNP is more rigorous in its calculations but the tradeoff is much longer computational times. By comparing both GADRAS and MCNP results to identical experimental data, conclusions can start to be drawn about the circumstances when GADRAS simplifications are no longer sufficient and the additional computational cost of MCNP is warranted. Select criteria are repeated below from the GADRAS results report [7] for comparison. This

section is divided in to three sections: evaluation of peak areas, evaluation of the continuum, and a discussion of overall trends.

5.1. Peak Areas

Peak areas are the most important part of the spectrum for a model to get correct, when using a high-resolution detector. Peak areas are used to identify nuclides, estimate activity, and infer information about intervening materials.

The peak areas for the Co-60 configurations are shown in Table 10. For GADRAS, 53% of the peaks were within 5% of the measured data, and 71% were within 10%. The GADRAS peaks that were more than 5% from measured peak area were evenly divided between larger and smaller peak areas. For MCNP, 35% of the peaks within 5% of measured data, and 69% were within 10% of measured peak area. The MCNP peaks that were more than 5% from measured data tended to be larger than measured peak area. Averaging the percent difference between the two peaks gives a single value to compare the peak area fit between the two models. Both models had an average percent difference over 10% for several configurations: the lead+MHE sphere and the far ends of the offset configurations, 150 and 200 cm, with the exception of Right-150 for MCNP, which was just below 10%. In one case, MCNP was within 10% on the measured and GADRAS was not: the large source behind a shield. There was also one case where GADRAS was within 10% and MCNP was not: the polyethylene-iron sphere.

Table 10. Comparison of Peak Area Fit for Co-60 Configurations between Measured and Synthetic Spectra for Both GADRAS and MCNP

Config	% Difference, 1173 keV peak		% Difference, 1332 keV peak		Average % Difference, both peaks	
	GADRAS	MCNP	GADRAS	MCNP	GADRAS	MCNP
Fe box	-3.4%	2.4%	-3.0%	6.1%	-3.2%	4.3%
Pb box	-3.5%	-9.9%	-2.6%	-4.9%	-3.1%	-7.4%
Pb sphere	-0.8%	-6.9%	-0.2%	-2.0%	-0.5%	-4.5%
Pb-MHE sphere	-13.2%	-25.0%	-10.0%	-19.8%	-11.6%	-22.4%
Left-200 cm	34.2%	11.4%	36.7%	18.4%	35.5%	14.9%
Left-150 cm	16.1%	7.1%	18.0%	13.6%	17.1%	10.3%
Left-100 cm	3.7%	5.2%	3.0%	10.2%	3.4%	7.7%
Left-50 cm	-1.9%	1.1%	-2.2%	6.6%	-2.0%	3.8%
Center	1.0%	-1.6%	-0.4%	2.6%	0.3%	0.5%
Right-50 cm	-3.9%	-1.0%	-4.6%	4.0%	-4.2%	1.5%
Right-100 cm	2.1%	3.4%	3.5%	10.7%	2.8%	7.1%
Right-150 cm	12.9%	4.4%	16.7%	12.4%	14.8%	8.4%
Right-200 cm	34.1%	11.2%	38.8%	20.3%	36.5%	15.7%
Backscatter	2.7%	5.6%	2.7%	6.0%	2.7%	5.8%
Shielded	-5.1%	-8.4%	0.3%	-1.7%	-2.4%	-5.0%
Big Source Shielded	12.6%	6.9%	11.9%	9.8%	12.3%	8.3%
FePE	-6.7%	-4.6%	-6.2%	-3.2%	-6.4%	-3.9%
PEFe	-5.9%	31.1%	-5.8%	26.1%	-5.8%	28.6%
Co-60 unshielded	-0.4%	-6.8%	0.1%	-1.7%	-0.1%	-4.3%
Co-60 2.5" PE	-5.0%	-6.6%	-4.6%	-1.9%	-4.8%	-4.3%
Co-60 3.5" PE	-4.7%	-5.9%	-4.0%	-0.7%	-4.3%	-3.3%

Co-60 4.5" PE	-6.2%	-7.0%	-5.2%	-1.7%	-5.7%	-4.4%

In the case of Cf-252, both GADRAS and MCNP did not correctly include the 388 keV peak from Cf-249. This is likely due to aging not being accounted for properly, as this peak appears to grow in with age. In the unshielded case, neither GADRAS nor MCNP properly predicted the 2223 keV peak from neutron interactions with hydrogen, likely because there was no explicit hydrogen in the models for interaction. These interactions primarily arise from other environmental sources that were not explicitly included in the model. GADRAS continued the trend of poorly predicting neutron interactions with the increasing polyethylene shielding. MCNP, however, predicted the 2223 keV peak within 6% for all three thicknesses of polyethylene, not significantly worse than the average performance for the Co-60 peak area predictions.

Table 11. Comparison of Peak Area Fit for Cf-252 Configurations between Measured and Synthetic Spectra for Both GADRAS and MCNP

Config	% Difference, 388 keV peak		% Difference, 2223 keV peak	
	GADRAS	MCNP	GADRAS	MCNP
Cf-252 unshielded	No peak	-90.5%	No peak	-61.6%
Cf-252 2.5" PE	No peak	No peak	-68.9%	-5.4%
Cf-252 3.5" PE	No peak	No peak	-70.2%	-0.5%
Cf-252 4.5" PE	No peak	No peak	-38.7%	5.1%

For the depleted uranium cases, only one was modeled with MCNP. Due to challenges discussed previously (Section 4.6), the other configurations were not modeled with MCNP, and the configuration that was modeled produced peaks that were over 30% too large. The synthetic peak areas relative to the experimental data are shown in Table 12. The 1001 keV peak was satisfactory in all the GADRAS spectra. The 186 keV is a much smaller peak and is at low energy. The GADRAS models generated a 186 peak that was 9% high for the 4 inch sphere and 12% low for the 6 inch sphere. There is not a significant peak at 186 keV with the 6 inch DU sphere in iron.

Table 12. Comparison of Peak Area Fit for DU Configurations between Measured and Synthetic Spectra for Both GADRAS and MCNP

Config	% Difference, 186 keV peak		% Difference, 1001 keV peak	
	GADRAS	MCNP	GADRAS	MCNP
DU 4"	9.2%	36.5%	-2.4%	33.9%
DU 6"	-12.4%	No model	-3.4%	No model
DU 6" + Fe 1.25"	No peak	No model	-2.3%	No model

5.2. Continuum

MCNP consistently underestimated the continuum for all Co-60 configurations and GADRAS generally overestimated the continuum. Table 13 shows the comparisons. Just over half of the GADRAS Co-60 configurations and just under a quarter of the MCNP Co-60 configurations have an average percent difference less than 10%. Almost 70% of the GADRAS and about 80% of the MCNP Co-60 configurations have an average percent difference less than 20%. The GADRAS configurations with an average percent difference more than 20% are the iron box and the offset configurations at 100 cm or more with the fit getting progressively worse with increasing offset. Surprisingly, the MCNP had greater than 20% average percent difference for both bare line-of-sight configurations (the center of the offset series and

the unshielded source from the increasing thickness series) as well as the backscatter configuration and the thinnest polyethylene shield.

Table 13. Comparison of Continuum Fit for Co-60 Configurations between Measured and Synthetic Spectra for Both GADRAS and MCNP

Config	Average % Difference		% More than 3 σ Difference	
	GADRAS	MCNP	GADRAS	MCNP
Fe box (AD=80)	27.7%	-6.4%	41.1%	17.5%
Pb box (AD=58)	16.5%	-17.7%	38.5%	52.2%
Pb sphere (AD=58)	-9.1%	-18.7%	19.2%	59.7%
Pb-MHE sphere (AD=47.6)	8.0%	-18.7%	35.8%	93.4%
Left-200 cm	66.8%	-6.2%	32.2%	3.2%
Left-150 cm	48.5%	-10.5%	25.2%	3.6%
Left-100 cm	22.5%	-14.5%	7.7%	4.7%
Left-50 cm	5.4%	-18.2%	2.1%	7.2%
Center	4.1%	-22.4%	2.2%	12.9%
Right-50 cm	4.2%	-19.7%	2.3%	8.8%
Right-100 cm	21.9%	-16.0%	8.2%	5.0%
Right-150 cm	49.4%	-12.6%	26.7%	4.2%
Right-200 cm	76.3%	-7.7%	42.6%	3.0%
Backscatter	1.3%	-20.8%	14.6%	24.1%
Shielded	-4.4%	-5.0%	22.8%	14.1%
Big Source Shielded	-14.3%	-13.5%	35.9%	57.3%
FePE	8.0%	-10.0%	6.2%	4.6%
PEFe	16.2%	17.8%	13.7%	2.6%
Co-60 unshielded	-0.9%	-26.7%	2.2%	43.9%
Co-60 2.5" PE	1.6%	-20.8%	3.1%	28.5%
Co-60 3.5" PE	1.6%	-19.5%	3.5%	27.3%
Co-60 4.5" PE	2.3%	-17.6%	3.4%	22.0%

The continuum fits for both MCNP and GADRAS are worse for Cf-252 than Co-60 due to the complexity of the Cf-252 spectrum from the neutron interactions. GADRAS generally predicted neutron interaction gammas poorly, while MCNP was able to predict some interactions. The large amount of noise in the measured data makes additional comparisons challenging.

As mentioned previously, only one depleted uranium configuration was run in MCNP. It did not perform as well as GADRAS on that configuration, due to the difficulties in producing the model. GADRAS spectra showed a good fit in the continuum for all three cases. The results are shown in Table 14.

Table 14. Comparison of Continuum Fit for DU Configurations between Measured and Synthetic Spectra for Both GADRAS and MCNP

Config	Average % Difference		% More than 3 σ Difference	
	GADRAS	MCNP	GADRAS	MCNP
DU 4"	6.1%	20.6%	1.5%	10.7%
DU 6"	-0.1%	No model	3.6%	No model
DU 6" + Fe 1.25"	-0.2%	No model	1.5%	No model

5.3. Discussion

In many of the test configurations, GADRAS performed satisfactorily. In cases where it does not, MCNP sometimes would provide a better model, but several of the shortfalls are shared by both methods.

MCNP can handle offsets beyond 15° much better than GADRAS. To generate the best response function in GADRAS, the detector parameters are often altered somewhat from the physical values. This makes the head-on empirical fit better but results in poor performance when the source is not directly in front of the detector.

For cases with multiple layered shielding material where GADRAS does not always predict the transport correctly, MCNP does not consistently do better. Multiple materials in series seem to be a challenge for both codes, but the results may be good enough for many purposes if there is sufficient measured data to benchmark against.

Neutrons are a challenge, particularly when there are likely interactions in the environment that are not accounted for in the model. GADRAS poorly predicted the hydrogen capture and many other neutron interactions that were not explicitly investigated. MCNP performed much better, with hydrogen capture consistent with the measured data. MCNP, too, did not predict all the interaction gammas.

GADRAS does quite well with bare or somewhat shielded depleted uranium directly in the detector's field of view. No challenging configurations were measured with the depleted uranium, which we would expect to show similar trends in goodness-of-fit to the Co-60 examples.

6. Conclusions

MCNP performed reasonably well with the Co-60 and Cf-252 configurations. It did poorly with the DU configurations due to the complexity and expense of allowing it to converge.

GADRAS 18.7.9 performed reasonably well for configurations in the direct line of sight of the detector with gamma only sources whose strengths were close to those used to generate the response function, without complex layered shielding.

The additional computational expense for MCNP would be justified in configurations where the source is not in direct line of sight (off angle), neutron-induced gammas are significant or source strength is much different from those used to generate the response function. However, care should be taken if small features in the low energy range must be generated with precision as it generally fit the low energy range poorly.

7. References

[1] C.J. Werner (editor), "MCNP Users Manual - Code Version 6.2", LA-UR-17-29981 (2017).
[2] Horne, Steven M., Thoreson, Gregory G, Theisen, Lisa A., Mitchell, Dean J., Harding, Lee, and Amai, Wendy A. GADRAS-DRF 18.5 User's Manual.. United States: N. p., 2014. Web. doi:10.2172/1166695.
[3] Hau, I.D., Russ, W.R., & Bronson, F. (2009). MCNP HPGe detector benchmark with previously validated Cyltran model. *Applied Radiation and Isotopes, 67*(5), 711.

[4] Boson, Ågren, & Johansson. (2008). A detailed investigation of HPGe detector response for improved Monte Carlo efficiency calculations. *Nuclear Inst. and Methods in Physics Research, A, 587*(2-3), 304-314.
[5] Sangaroon, S., Wichaisri, W., Ratanatongchai, C., Picha, R., Khaweerat, J., & Channuie. (2017). *Journal of Physics: Conference Series, 901*(1), 012133/1-012133/4.
[6] Livesay, Jake, Combs, Jason C, Margrave, Timothy E, and Miller, Ian J. Efficiency of TTAC's ORTEC IDM. United States: N. p., 2012. Web. doi:10.2172/1048166.
[7] Stults, Lombardi, James, Klasky (2019). Comparison of GADRAS Modeled Spectra to Measured Spectra Using GADRAS 18.7.9 to Benchmark Modeling Limitations. LA-CP-19-20042.

8. Acknowledgements

"This research used resources provided by the Los Alamos National Laboratory Institutional Computing Program, which is supported by the U.S. Department of Energy National Nuclear Security Administration under Contract No. 89233218CNA000001."